Inorganic Chemistry

Article

pubs.acs.org/IC

Enhanced Photocatalytic Activity of α-Methylstyrene Oligomerization through Effective Metal-to-Ligand Charge-Transfer Localization on the Bridging Ligand

Hiroyuki Nitadori,[†] Takeshi Takahashi,[†] Akiko Inagaki,*[,†,‡] and Munetaka Akita*[,†]

[†]Chemical Resources Laboratory, Tokyo Institute of Technology, R1-27, 4259 Nagatsuta Midori-ku Yokohama 226-8503, Japan

[‡]Precursory Research for Embryonic Science and Technology (PRESTO), Japan Science and Technology Agency (JST), 4-1-8 Honcho, Kawaguchi, Saitama 332-0012, Japan

Supporting Information

ABSTRACT: A series of Pd complexes containing a visible-light harvesting moiety with various combination of substituents (R, X) were synthesized. The variation of the substituents resulted in significant change in the electrochemical and photophysical properties of the complexes. Additionally, photocatalytic activity drastically increased through the introduction of an electron-donating group on R and an electron-withdrawing group on X, respectively. The molecular orbital analysis based on density functional theory (DFT) calculation suggested that the enhancement of the catalytic activity is due to the effective Metal-to-Ligand Charge-Transfer (MLCT) localization on the bridging ligand.

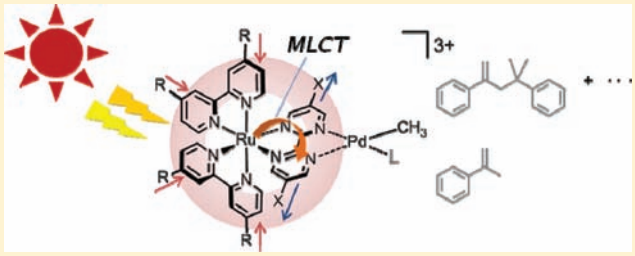

1. INTRODUCTION

The use of solar energy in the production of useful chemicals is important with respect to environmental protection because heavy use of fossil fuels is causing serious problems such as global climate change, diffusion of various environmental pollutants, and depletion of natural resources.[1] In nature, plants use sunlight extremely efficiently through photosynthesis.[2] Since reserves of fossil fuels are limited, it will be necessary for us to use natural sources of energy, mainly solar energy, as plants do. Researchers are therefore now involved in studying ways of using solar energy efficiently in a broad range of research areas.[3] In the field of coordination chemistry, many reports of photoactive metal complexes have been published.[4] Ru(II)−polypyridyl complexes, in particular, have been widely used as a photoactive component in a variety of systems because they show favorable physical properties such as long excited-state lifetimes and high luminescent efficiencies.[5] Although photophysical processes related to photosynthesis, such as photoinduced electron/energy transfer and formation of charge-separated states, have been much studied using finely designed model complexes, there have been far fewer studies of photocatalysis.[6] Research into highly efficient molecular transformations using inexhaustible visible-light energy may contribute to the future evolution of materials production.

We have been working on the photochemical conversion of organic molecules using transition-metal catalysts containing Ru(II)−polypyridyl derivatives as a visible-light-absorbing unit.[7] Systematic studies of the effects of substituents (X) in the 2,2′-bipyrimidine (bpm) bridging ligand on photocatalytic activities have shown that the introduction of suitable substituents drastically increases the photocatalytic activity as a result of effective Metal-to-Ligand Charge-Transfer (MLCT) transitions to the bridging ligand.[8] Thus, the combined effects of substituents R in the bipyridyl ligand, which constitutes the Ru(II) light-absorbing unit, with that of the bridging ligand (X) could lead to further reactivity enhancements. Here, we report the synthesis of novel Ru−Pd complexes with various combinations of substituents (R and X); the photophysical properties and catalytic reactivities of these complexes toward α-methylstyrene are also reported.

2. RESULT AND DISCUSSION

Preparation. The synthetic routes for the mononuclear Ru complexes, $[(bpy^R)_2Ru(bpm^X)]^{2+}$, and the corresponding Ru−Pd dinuclear complexes, $[(bpy^R)_2Ru(bpm^X)PdMe(solv.)]^{3+}$, are shown in Scheme 1. Most of the complexes, except for **2b** and **3b**, were formed by refluxing the dichloride precursor with bipyrimidine ligands according to the published method for the synthesis of **1a** (method A).[9] Complexes **2b** and **3b** were unable to be synthesized via method A. They were successfully synthesized through method B in which AgOTf and dibromobipyrimidine were added sequentially. Both complexes seem to be thermodynamically unstable and thus relatively mild conditions were needed for the synthetic procedure. On the other hand, various attempts to synthesize mononuclear Ru complexes containing the substituents R = NMe_2, X = Br, and R = OMe_2, X = Br were unsuccessful.

Received: February 18, 2011
Published: December 5, 2011

   dx.doi.org/10.1021/ic200291t | *Inorg. Chem.* 2012, 51, 51−62

Scheme 1. Synthetic Routes for $[(bpy^R)_2Ru(bpm^X)](BF_4)_2$ and $[(bpy^R)_2Ru(bpm^X)PdMe(Me_2CO)](BF_4)_3$

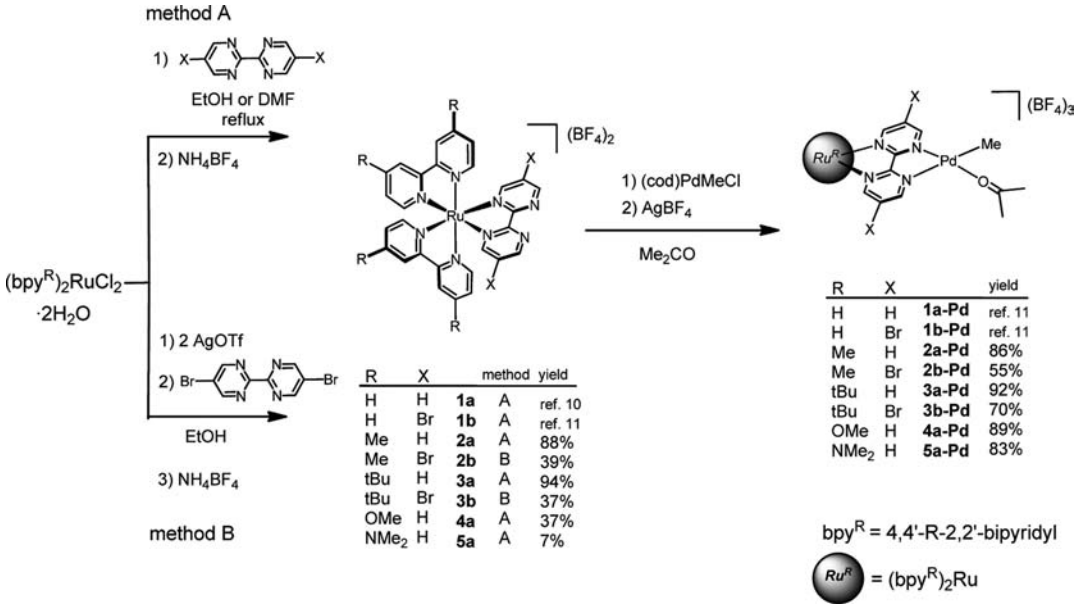

R	X		method	yield
H	H	**1a**	A	ref. 10
H	Br	**1b**	A	ref. 11
Me	H	**2a**	A	88%
Me	Br	**2b**	B	39%
tBu	H	**3a**	A	94%
tBu	Br	**3b**	B	37%
OMe	H	**4a**	A	37%
NMe_2	H	**5a**	A	7%

R	X		yield
H	H	**1a-Pd**	ref. 11
H	Br	**1b-Pd**	ref. 11
Me	H	**2a-Pd**	86%
Me	Br	**2b-Pd**	55%
tBu	H	**3a-Pd**	92%
tBu	Br	**3b-Pd**	70%
OMe	H	**4a-Pd**	89%
NMe_2	H	**5a-Pd**	83%

Table 1. Crystallographic Data

	2a	2b	3b	4a	2a-Pd
formula	$C_{38}H_{43}B_2F_8N_9ORu$	$C_{33}H_{30}N_8Br_2P_2F_{12}RuCl_2$	$C_{48}H_{62}B_2F_8N_8Br_2ORu$	$C_{32}H_{30}B_2F_8N_8O_4Ru$	$C_{41}H_{45}B_3F_{12}N_{12}PdRu$
formula weight	916.50	1160.38	1201.57	865.33	1173.79
crystal system	triclinic	triclinic	triclinic	triclinic	triclinic
space group	$P\bar{1}$ (#2)	$P\bar{1}$ (#2)	$P\bar{1}$ (#2)	$P\bar{1}$ (#2)	$P\bar{1}$ (#2)
a/Å	10.7067(11)	10.912(3)	10.866(6)	9.810(3)	11.8159(16)
b/Å	14.162(3)	14.096(8)	16.183(9)	11.656(6)	11.8722(16)
c/Å	14.449(3)	14.207(8)	18.127(6)	16.399(8)	19.5212(18)
α/deg	113.349(4)	106.397(11)	101.79(3)	74.678(13)	99.518(6)
β/deg	92.674(11)	101.67(3)	106.73(3)	79.78(3)	102.89(3)
γ/deg	96.639(10)	96.52(3)	109.361(14)	85.98(3)	108.866(4)
V/Å^3	1987.6(6)	2018.8(17)	2717(2)	1779.3(14)	2530.3(5)
Z	2	2	2	2	2
$d_{calc.}$/g cm^{-3}	1.531	1.909	1.469	1.615	1.541
temperature /°C	−60	−60	−60	−60	−60
radiation	MoKα (λ = 0.71069 Å)	MoKα (λ = 0.71069 Å)	MoKα (λ = 0.71069 Å)	MoKα (λ = 0.71069 Å)	MoKα (λ = 0.71069 Å)
μ/mm^{-1}	0.477	2.674	1.829	0.533	0.741
diffractometer	Rigaku RAXIS IV	Rigaku RAXIS IV	Rigaku RAXIS IV	Rigaku RAXIS IV	Rigaku RAXIS IV
max 2θ /deg	55.0	55.0	55.0	55.0	55.0
reflections collected	15432	15577	17608	12771	20691
independent	8149	8293	10 628	7127	10 549
reflections	[R(int) = 0.0536]	[R(int) = 0.158]	[R(int) = 0.0941]	[R(int) = 0.0851]	[R(int) = 0.0599]
no. of parameters refined	496	513	619	498	559
R1 ($I > 2\sigma$) %	6.28	7.40	6.98	8.78	6.57
wR_2 ($I > 2\sigma$) %	17.58	15.32	16.56	22.42	19.75
goodness of fit	1.047	0.838	0.870	1.077	1.094

Introduction of the Pd fragment was easily achieved in high yields for all the corresponding complexes using the procedure already reported by our group.[8,10] All the newly synthesized complexes were unambiguously identified on the basis of NMR and ESI-MS spectroscopy and some of the molecular structures have been clarified by single-crystal X-ray diffraction studies.

Molecular Structures. The molecular structures of the mononuclear Ru complexes **2a**, **2b**, **3b**, **4a**, and the Ru−Pd dinuclear complex **2a-Pd** were determined by single-crystal X-ray diffraction studies; the crystallographic data are collected in Table 1, and ORTEP diagrams of the cationic parts of the complexes are shown in Figure 1. Selected bond lengths and angles are listed in Table 2 along with those of the reference compounds **1a** and **1b** for comparison. The Ru centers of all the complexes possess a slightly distorted octahedral geometry similar to that of the previously reported complex **1a**.[9] The Ru−N bond lengths and N−Ru−N chelate angles of the diimine ligands are similar in all the complexes. The data indicate that the introduction of substituents at the 4,4′-positions of the bipyridyl ligand as well as at the 5,5′-position of

dx.doi.org/10.1021/ic200291t | Inorg. Chem. 2012, 51, 51−62

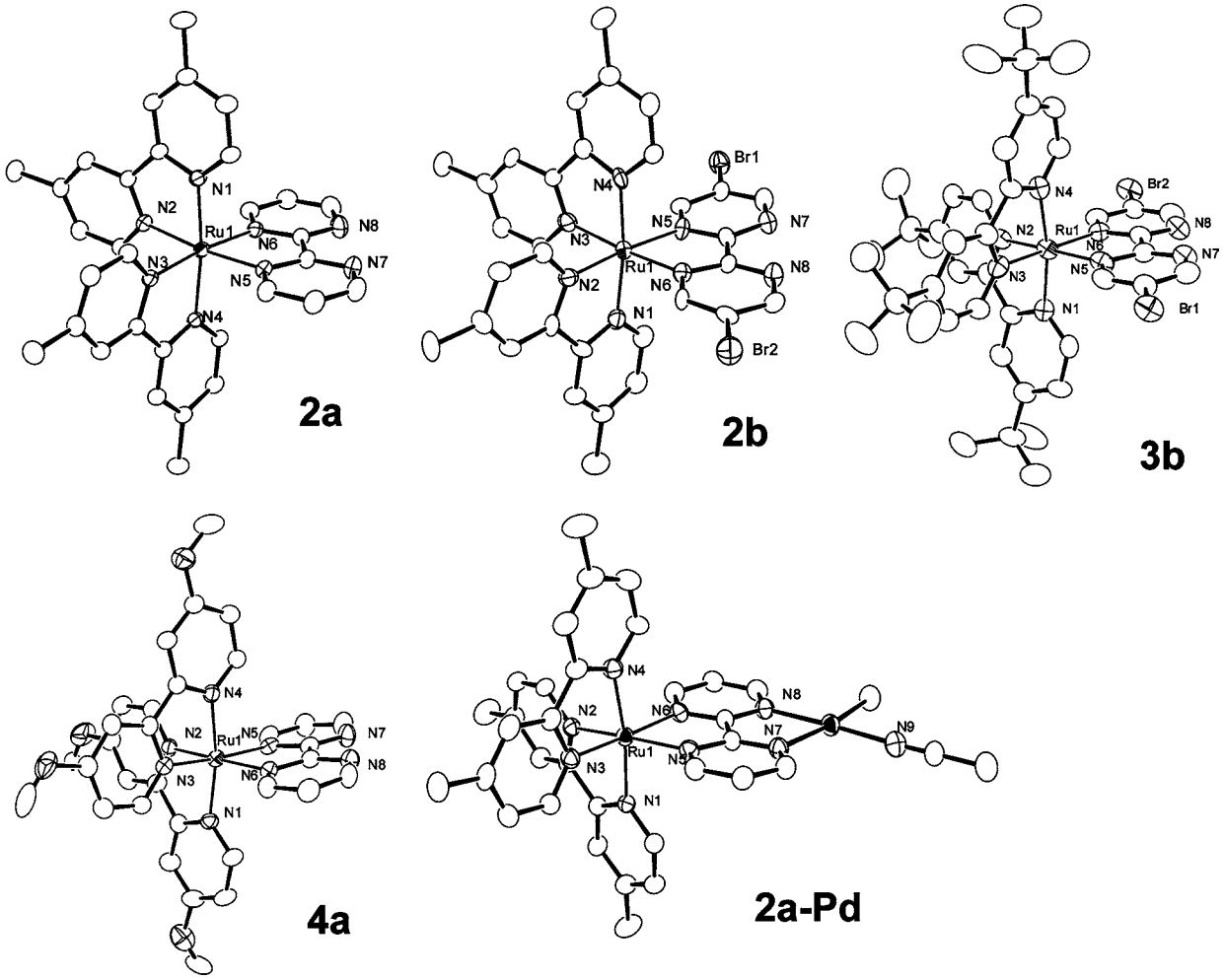

Figure 1. ORTEP diagrams of the cationic parts of **2a**, **2b**, **3b**, **4a**, and **2a-Pd**. Non-H atoms are represented by ellipsoids at the 30% probability level. Hydrogen atoms have been omitted for clarity.

Table 2. Selected Bond Lengths (Å) and Angles (deg)

	1a[a]	1b[b]	2a	2b	3b	4a	2a-Pd
Ru–N1	2.041(6)	2.102(9)	2.070(3)	2.059(11)	2.037(8)	2.092(5)	2.071(4)
Ru–N2	2.064(6)	2.076(9)	2.069(3)	2.042(9)	2.015(7)	2.069(5)	2.056(5)
Ru–N3	2.066(7)	2.083(9)	2.069(3)	2.082(11)	2.064(8)	2.060(5)	2.079(4)
Ru–N4	2.064(7)	2.093(9)	2.065(3)	2.046(10)	2.046(7)	2.074(5)	2.075(4)
Ru–N5	2.061(6)	2.056(8)	2.066(3)	2.061(9)	2.040(8)	2.051(5)	2.079(5)
Ru–N6	2.062(6)	2.097(9)	2.061(3)	2.023(9)	2.054(7)	2.058(5)	2.080(4)
Ru–N(bpy) (av.)	2.058	2.089	2.068	2.057	2.041	2.074	2.070
Ru–N(bpm) (av.)	2.062	2.077	2.064	2.042	2.047	2.055	2.080
Ru–N(av.)	2.060	2.085	2.067	2.052	2.042	2.067	2.073
N1–Ru–N2	78.8(3)	78.8(4)	78.36(13)	79.7(4)	78.3(3)	78.31(18)	78.44(17)
N3–Ru–N4	79.1(3)	78.8(4)	78.33(13)	78.5(4)	78.9(3)	78.34(18)	78.50(18)
N5–Ru–N6	78.6(3)	78.2(4)	78.51(13)	78.5(4)	79.3(3)	78.50(18)	79.37(17)
N–Ru–N(av.)	78.8	78.6	78.40	78.9	78.8	78.4	78.77

[a]Ref 9. [b]Ref 8.

the bipyrimidine ligand do not cause steric hindrance of the octahedral geometry of the Ru center. In the case of the dinuclear Ru–Pd complex, **2a-Pd**, the structural parameters of the Ru center are also similar to those of **1a** and **2a**. This also suggests that the introduction of the Pd–alkyl fragment does not have steric effects on the chromophore unit. The hindered geometry, which may originate from steric repulsion between or within the diimine ligands, results in preferential thermodynamic quenching of the photoexcited state, which is an undesirable property in light-absorbing units.

Reactivity Studies. We have been studying the photochemical reactions of alkenes with Pd catalysts containing various visible-light sensitizers.[8,10,11] α-Methylstyrene was selectively dimerized by visible-light irradiation of a solution containing a catalytic amount of a Ru–Pd catalyst to give 2,4-diphenyl-4-methyl-1-pentene in high yield (eq 1). A reaction

dx.doi.org/10.1021/ic200291t | Inorg. Chem. 2012, 51, 51–62

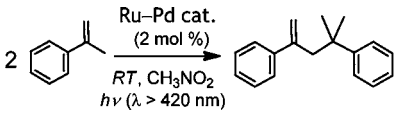

(1)

mechanism based on various control experiments was also presented. The rate-determining step in the catalytic cycle was the second insertion of α-methylstyrene into a Pd−CMe_2Ph species (**C**), and light irradiation seemed to accelerate this insertion step (**C** → **D**) (Scheme 2).

Scheme 2. Rate-Determining Step in the Photocatalytic Reaction with α-Methylstyrene

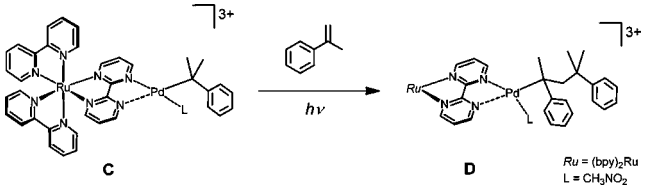

The reaction mechanism of formation of **C** from **1a-Pd** is as follows. Insertion of α-methylstyrene into the palladium-methyl bond gives the intermediate **A**, followed by C(β2) -H elimination results in the formation of the active-hydride intermediate **B** and 2-phenyl-2-butene, and then, reinsertion of α-methylstyrene into **B** yields **C** (Scheme 3, Supporting Information, Scheme S1). The intermediates **A**, **C** and 2-phenyl-2-butene have been fully characterized by NMR spectroscopy and MS spectrometry.[8]

Brookhart et al. have described a family of Pd(II) and Ni(II) complexes bearing bulky aryl-substituted α-diimine ligands which are capable of polymerizing ethylene, α-olefins, and internal and cyclic olefins.[12] The mechanistic and kinetic studies of the Pd(II)-alkyl complexes using NMR spectroscopic techniques have been carried out since the Pd(II) complexes are more easily synthesized and handled in contrast to the corresponding Ni(II) analogues. Each elementary reactions in the proposed reaction mechanism in the present paper (Schemes 2, 3, Supporting Information, Scheme S1), proceeded identically as the Pd(II)-diimine complexes reported by Brookhart et al.[13] Thus the mechanism catalyzed by the Pd(0) nanoparticles which may have formed via decomposition by light-irradiation can be excluded.

In a previous report, it was shown that the activity of the catalyst with a Br substituent on the bpm bridging ligand (**1b-Pd**) was much higher than that of the corresponding nonsubstituted catalyst (**1a-Pd**). Next, we considered the effects of the substituents in the bipyridyl ligand, two of the three diimine ligands which constitute the Ru(II) chromophore. We investigated the reaction with α-methylstyrene using catalysts with electron-donating substituents, such as Me, ^{t}Bu, OMe, and NMe_2 groups, on the bipyridyl ligands (eq 2). The

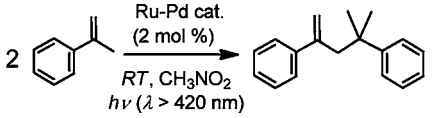

(2)

α-methylstyrene consumption rates using the catalysts synthesized in the previous section are plotted in Figure 2.

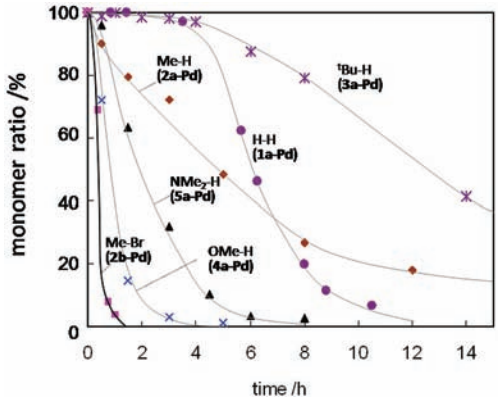

Figure 2. Consumption rate of monomer in the catalysis.

As can easily be seen from the figure, the introduction of electron-donating groups such as Me, OMe, and NMe_2 significantly shortened the induction period, and the total reaction time decreased drastically. Exceptionally, the reaction rate using the catalyst with a ^{t}Bu group (**3a-Pd**) was slower than that for **1a-Pd**. The catalytic activity enhancement can be interpreted as preferential MLCT transitions to the bpm ligand, but the reduction in the excited-state lifetime caused by the bulky ^{t}Bu group results in decreased catalytic activity.

The combined effects of the substituents in the bipyridyl and bipyrimidine ligands may contribute to further enhancement. On this basis, we next investigated the reaction of the Me−Br-substituted catalyst **2b-Pd**, and found that it showed the highest photocatalytic activity (Figure 2, bold line). The main product in the photocatalysis was a methylstyrene dimer, but trimers

Scheme 3. Plausible Mechanism of Formation of C

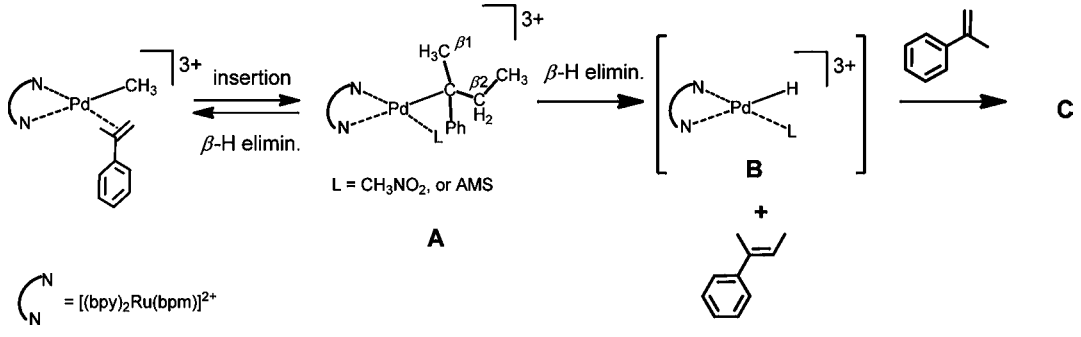

dx.doi.org/10.1021/ic200291t | Inorg. Chem. 2012, 51, 51−62

and tetramers were also formed.[14] The product distribution seems to depend on the reactivity of the catalyst since reactions with catalysts with higher reactivities tend to give more trimers and tetramers. It seems that the dimers formed react again with the catalyst to give products with higher degrees of oligomerization.

Electrochemical Properties. To clarify the electrochemical properties of the complexes, cyclic voltammogram (CV) measurements were conducted in CH_3CN solution under ambient conditions using a Pt electrode. The cyclic voltammograms of the mononuclear complexes are shown in Figure 3,

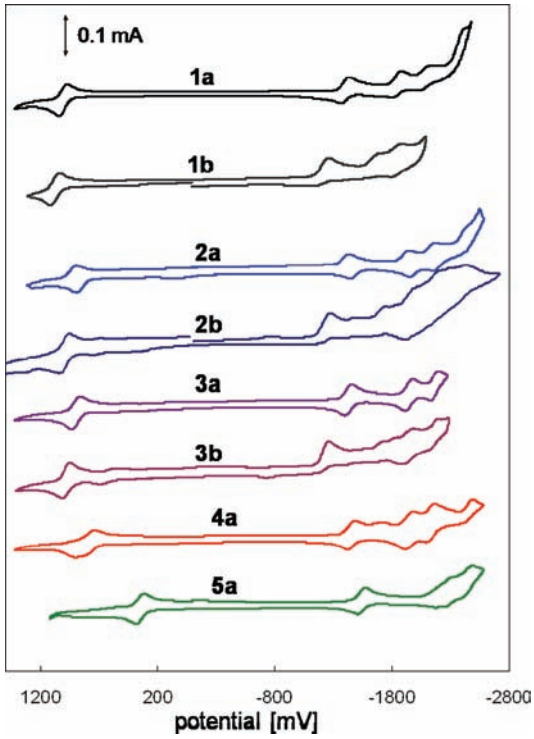

Figure 3. Cyclic voltammograms of mononuclear Ru complexes.

and the redox potentials are summarized in Table 3. Redox data for **1b-Pd**, **2b-Pd**, and **3b-Pd** are not shown in the table because the dinuclear complexes with a 5,5′-dibromo-2,2′-bipyrimidine ligand are electrochemically too unstable to detect redox currents in the CV measurements.

In the cyclic voltammograms of the mononuclear Ru complexes, the single reversible or quasi-reversible wave in the anodic region can be assigned to a metal-centered oxidation process ($Ru^{II/III}$).[15,16] The three waves in the cathodic region are assigned to one-electron reduction processes of the bipyrimidine and bipyridyl ligands; that of bipyrimidine has the most positive potential.[16] In the case of the dinuclear Ru−Pd complexes, a second reduction wave of the bipyrimidine ligand ($bpm^{-1/-2}$) was observed within the potential window because of the reduced electron density as a result of introduction of the cationic Pd fragment.[6b]

For the series of mononuclear Ru complexes, comparison of the values for **1a**, **2a**, and **3a** with those for **1b**, **2b**, and **3b**, respectively, showed that introduction of a bromo substituent led to an anodic shift of the $E(bpm^{0/-1})$ value of about 0.2 V, from −1.4 V to −1.2 V, although all the Br-substituted complexes showed irreversible couples (Table 3, Figure 3). The reason of the anodic shift is the relatively large Hammett constant of the Br substituent ($\sigma_{meta}(Br) = 0.391$), which is effective in reducing the electron density of the bipyrimidine ligand. Electron-donating substituents in the bipyridyl ligand, from H, Me, ^{t}Bu, OMe, to NMe_2, resulted in cathodic shifts of the $E(Ru^{II/III})$ values from 1.0 to 0.35 V, and anodic shifts of the $E(bpy^{0/-1})$ values; this also suggest increased electron density at the Ru center. Similar substituent effects on the redox potential shifts were observed in the series of corresponding Ru−Pd dinuclear complexes. The marked changes in the redox potentials caused by introducing various substituents may result in the energetic changes in the frontier molecular orbitals. The related theoretical data will be discussed in a later section.

Photophysical Properties. UV−vis absorption and emission data of the reference compounds, $[Ru(bpy)_3]^{2+}$ and $[(bpy)_2Ru(bpm)]^{2+}$, and those of the series of mononuclear Ru complexes and the corresponding Ru−Pd dinuclear complexes are summarized in Table 4. All the data were collected in CH_3CN solution at ambient temperature. The emission data were measured by irradiating a normalized sample (O.D.(λ = 450 nm) = 0.1), and the intensities are shown as relative values versus $[Ru(bpy)_3]^{2+}$. The data for the dinuclear complexes were also compared with the data for the corresponding mononuclear complexes, and the values are shown in parentheses.

UV−vis spectra of the mononuclear Ru complexes with various substituents are shown in Figure 4. Spectra of the corresponding dinuclear Ru−Pd complexes are provided in the Supporting Information, Figure S1. All the complexes exhibit MLCT absorptions around 450 nm, attributable to the d(Ru) → π^* transition.[16,17] Mononuclear complexes with electron-donating substituents, such as **2a**, **3a**, **4a**, and **5a**, showed a shoulder peak in addition to the characteristic MLCT absorption, similar to that seen in the reference compounds. Introduction of a bromo substituent (**2a** vs **2b**, **3a** vs **3b**) led to a blue-shift and a red-shift of the MLCT main peak and the shoulder peak, respectively. These changes can be interpreted as splitting of the single MLCT band into two (metal-to-bpy and metal-to-bpm charge-transfer) because the MO levels of bipyridyl and bipyrimidine have become larger as a result of the modification. The MLCT band in the longer wavelength region should be assigned to the metal-to-bpm charge transfer band.[16,17] Introduction of Me and ^{t}Bu substituents gives rise to shoulder peaks, and the further introduction of the Br substituent brings about marked splitting of the MLCT band. The NMe_2- and OMe-substituted complexes **4a** and **5a** exhibit a broad, split MLCT band. The Ru(II)−diimine complexes exhibit a relatively narrow $\pi-\pi^*$ absorption band at around 280 nm, but the bands of complexes **4a** and **5a** are characteristically broader and split in this region.

Figure 5 provides a comparison of the spectra of the corresponding mono- and dinuclear complexes (**2b** vs **2b-Pd**, **5a** vs **5a-Pd**). The UV−vis absorption spectra of the dinuclear complexes were almost identical to those of the mononuclear complexes other than a slight decrease in the molar absorptivity. Unlike the drastic changes observed in the CV data as a result of dinucleation, only a slight change was observed in the UV−vis absorption spectra. We do not know the exact reason for these phenomena, but the introduction of the Pd fragment may have an equal influence on the energy levels of the MOs with respect to the ^{1}MLCT, which results in the spectra of the mono- and dinuclear complexes being almost the same.

Ru complexes with a bipyrimidine ligand exhibit phosphorescence, which originates from the triplet excited-state.

dx.doi.org/10.1021/ic200291t | Inorg. Chem. 2012, 51, 51−62

Table 3. Redox Properties[a]

	$E_{1/2}$				
complex (R–X)[b]	$Ru^{II/III}$	$bpm^{0/-1}$	$bpm^{-1/-2}$	$bpy^{0/-1}$	$bpy^{0/-1}$
$[Ru(bpy)_3](BF_4)_2$	0.88 (55)			−1.74 (62)	−1.93 (54)
1a (H–H)	1.00 (68)	−1.40 (90)		−1.85 (91)	−2.14 (90)
1b (H–Br)	1.08 (80)	−1.21 (86)		−1.72(irr)	−1.87 (90)
2a (Me–H)	0.90 (68)	−1.44 (58)		−1.89 (70)	−2.09 (70)
2b (Me–Br)	0.99 (92)	−1.27 (irr)		−1.97(142)	−2.19 (132)
3a (^{t}Bu–H)	0.89 (64)	−1.43 (64)		−1.95 (64)	−2.18 (46)
3b (^{t}Bu–Br)	0.98 (66)	−1.20 (122)		−1.93 (96)	−2.15 (74)
4a (OMe–H)	0.77 (76)	−1.46 (64)		−1.95 (66)	−2.13 (78)
5a (NMe_2–H)	0.35 (70)	−1.54 (64)		−2.28 (64)	−2.46 (70)
1a-Pd (H–H)Pd	1.26 (100)	−0.85 (126)	−1.54 (64)	−1.85 (112)	−2.16 (122)
2a-Pd (Me–H)	1.16 (98)	−0.89 (150)	−1.49 (irr)	−1.65 (irr)	−1.98 (134)
3a-Pd (^{t}Bu–H)	1.15 (99)	−0.89 (146)	−1.48 (irr)	−1.66 (irr)	−2.01 (90)
4a-Pd (OMe–H)	0.93 (55)	−0.98 (60)	−1.64 (100)	−2.02 (92)	−2.25 (96)
5a-Pd (NMe_2–H)	0.53 (58)	−1.05 (62)	−1.56 (82)	−1.76 (76)	−2.38 (irr)

[a]Measurements were carried out in CH_3CN with 0.1 M $[Bu_4N]BF_4$ *V* vs *E* (Fc/Fc^+). The numbers in parentheses are the differences (mV) between the anodic and cathodic waves. irr stands for an irreversible redox wave. [b](R–X) represents the substituents on the bipyridyl (R) and bipyrimidine ligands (X).

Table 4. Photophysical Data[a]

	absorption[c]		emission[d]	
complex (R–X)[b]	λ_{max}/nm	$\varepsilon/10^4$ M^{-1} cm^{-1}	λ_{em}/nm	Φ_{rel}[e,f]
$[Ru(bpy)_3](PF_6)_2$	452	1.40	596	1
1a (H–H)	423	1.20	599	0.05
1b (H–Br)	416, 498 (sh)	1.40, 0.57 (sh)	600	0.11
2a (Me–H)	423, 483 (sh)	1.10, 0.54 (sh)	600	0.029
2b (Me–Br)	414, 511 (sh)	1.52, 0.49 (sh)	600, 664	0.11
3a (^{t}Bu–H)	421, 482 (sh)	1.40, 0.62 (sh)	604	0.009
3b (^{t}Bu–Br)	414, 515 (sh)	1.45, 0.43 (sh)	659	0.11
4a (OMe–H)	425, 503 (sh)	1.02, 0.48 (sh)	668	0.011
5a (NMe_2–H)	431, 570 (sh)	1.62, 0.36 (sh)	621	0.017
1a-Pd (H–H) Pd	425	1.70	634	0.03 (0.60)
2a-Pd (Me–H) Pd	421, 481 (sh)	1.40, 0.70 (sh)	656	0.01 (0.34)
3a-Pd (^{t}Bu–H) Pd	420, 482 (sh)	1.80, 0.73 (sh)	657	0.006 (0.67)
4a-Pd (OMe–H) Pd	428, 507 (sh)	1.38, 0.57 (sh)	676	0.007 (0.64)
5a-Pd (NMe_2–H) Pd	431, 569 (sh)	1.50, 0.33 (sh)	620	0.013 (0.76)

[a]Measurements were carried out in CH_3CN at room temperature. [b](R–X) represents the substituents on the bipyridyl (R) and bipyrimidine ligands (X). [c]sh indicates a shoulder peak. [d]λ_{ex} = 450 nm (O.D. = 0.1). [e]Luminescence intensity relative to $[Ru(bpy)_3]^{2+}$. [f]Numbers in parentheses represent luminescence intensity relative to the corresponding mononuclear complex.

However, the luminescent quantum yields of the series of bipyrimidine complexes ($[(bpy^R)_2Ru(bpm^X)]^{2+}$) decrease to about 5–10% of that of $[Ru(bpy)_3]^{2+}$. The presence of two sets of free lone-pairs, located close to each other, in the bpm ligand may cause electronic repulsion between the lone-pairs, resulting in promotion of thermodynamic quenching of the triplet excited-state. In addition, stabilization of the lowest unoccupied molecular orbital (LUMO) of bpm character reduces the energy gap between the highest occupied molecular orbital (HOMO) and LUMO; this contributes to faster nonradiative quenching, according to the energy-gap law. Within a series of mononuclear Ru–bpm complexes, introduction of bulky substituents such as a ^{t}Bu group tends to lower the luminescent quantum yields (Table 4). This may be a result of steric hindrance brought about by the octahedral geometry. In contrast, increased emission intensities were observed for the Br-bpm complexes; this may be caused by electron withdrawal of the bpm lone-pairs, resulting in less repulsion between them. Dinucleation by introduction of the Pd–Me moiety led to drastic reductions in the luminescent quantum yields compared with those of the corresponding mononuclear complexes. It implies that the electronic effect of the Pd moiety toward the bpm ligand is similar to those of the Br substituents. Additionally, the planarity of the bpm unit increases through Pd coordination. Both effects should contribute to an increase of emission intensity; however, energy transfer to the Pd center cancels out the effects and emission is significantly reduced.

A schematic representation of the molecular orbital energies based on the CV and UV–vis absorption data is shown in Figure 6. Here, we will focus on the MO energies of the

dx.doi.org/10.1021/ic200291t | *Inorg. Chem.* 2012, 51, 51–62

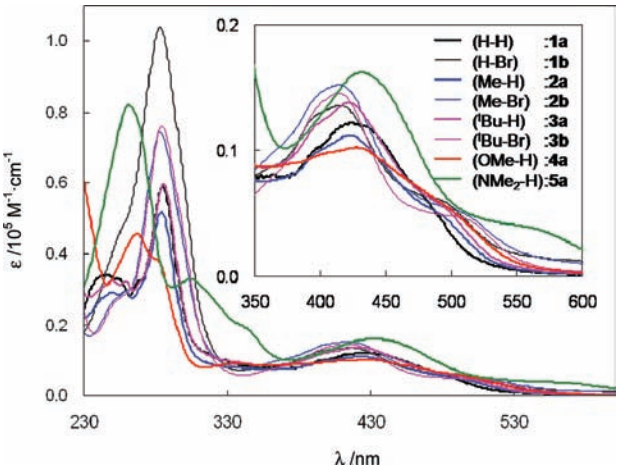

Figure 4. UV−vis spectra of mononuclear Ru complexes.

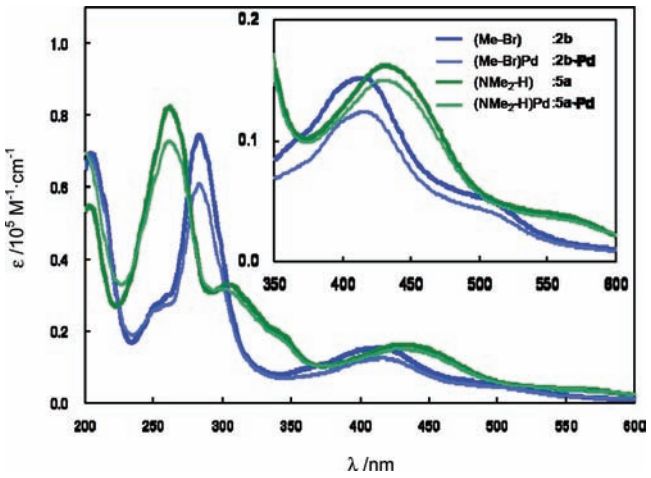

Figure 5. UV−vis spectra of **2b**, **2b-Pd**, **5a**, and **5a-Pd**.

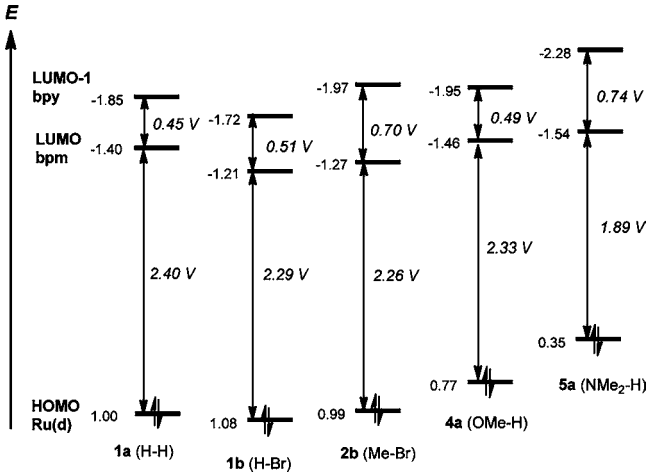

Figure 6. Schematic representation of MO energy levels of the frontier orbitals of **1a**, **1b**, **2b**, **4a**, and **5a**.

mononuclear Ru(II) complexes since clear CV data for the dinuclear complexes could not be obtained, and there were only slight differences between the UV−vis absorption data of the mononuclear and dinuclear complexes. The MO energies of **2a**, **3a**, and **3b** were omitted to simplify the comparison. In the cyclic voltammograms, the first redox wave in the anodic region was assigned to a $Ru^{II/III}$ process, and the first and second redox waves in the cathodic region were assigned to $bpm^{0/-1}$ and $bpy^{0/-1}$ processes. Thus, the HOMO, LUMO, and LUMO+1 orbitals are shown to possess Ru(d), bpm, and bpy characters, respectively.

Introduction of the electron-withdrawing Br group in bpm leads to marked stabilization of the LUMO (**1a** → **1b**), and introduction of the electron-donating Me group in bpy results in destabilization of the LUMO+1 (**1b** → **2b**). These modifications result in a drastic increase in the energy differences between the LUMO and the LUMO+1. Introduction of OMe and NMe_2 groups in bpy results in destabilization of the HOMO as well as of the LUMO+1. Since the ^{1}MLCT band mainly originates from d(Ru) → π^*(bpm) and d(Ru) → π^*(bpy) transitions, a reduction in the energy differences between the HOMO and the LUMO results in a red-shift of the band. An increase in the energy differences between the LUMO and the LUMO+1 leads to the appearance of shoulder peaks because of the two energetically different transitions. The MO energy changes based on the CV data correspond well with the UV−vis absorption spectral changes shown in the previous section.

Theoretical Studies. To clarify the substituent effects on the frontier orbital energies, we have examined the DFT calculations for a series of mononuclear complexes. The following basis sets were used in the ground-state geometry optimization using Gaussian 03[18] and 09[19] program packages: Lanl2DZ for Ru and Pd, 6-31G+ for N atoms coordinated to Ru, 6-31G for O in the methoxy group, and 3-21G for the other C, H, and N atoms. The Ru−N bond lengths and the chelate angles between Ru and the bpy and bpm ligands of the optimized structures reproduced the experimental results well, although the Ru−N bond lengths were longer by about 1−2%.

The molecular orbitals of the complexes, based on the theoretical calculations, are presented in Figure 7. For all the $[(bpy^R)_2Ru(bpm^X)]^{2+}$ mononuclear complexes, the HOMO had the Ru(d) orbital character, and the LUMO and the LUMO+1 had the bpm and bpy characters, respectively, in contrast to the LUMO of $[Ru(bpy)_3]^{2+}$ having the bpy character equally delocalized on the three bpy ligands. Thus, these orbitals should have the main contributions to the MLCT process. The introduction of an electron-withdrawing group in the bpm ligand (**1a** → **1b**) stabilizes the LUMO, and introduction of an electron-donating group in the bpy ligand (**1a** → **2a**, **4a**, **5a**) destabilizes the LUMO+1 orbital. The HOMO is also destabilized by this bipyridyl substitution; however, the extent of the effect is much smaller than that on the LUMO+1. Thus, the introduction of electron-donating and electron-withdrawing substituents in the bpy and bpm ligands results in the destabilization of the LUMO+1 and stabilization of LUMO. Although the qualitative values of the energy differences do not completely match with those of the CV data, these energy changes have good correlation with the MO analysis using the CV data (Figure 6).

The increase in the energy differences between the two orbitals leads to preferential MLCT to the stabilized bpm ligand. The MLCT transition to bpm enhances the photocatalytic reaction, so the highest photocatalytic activity of **2b-Pd** is a result of an MO energy change and the accompanying preferential MLCT to bpm. Introducing a strongly electron-donating NMe_2 or OMe group also leads to an increase in the energy difference between the LUMO and the LUMO+1. Thus the catalytic activities of **4a-Pd** and **5a-Pd** were higher than that

dx.doi.org/10.1021/ic200291t | Inorg. Chem. 2012, 51, 51−62

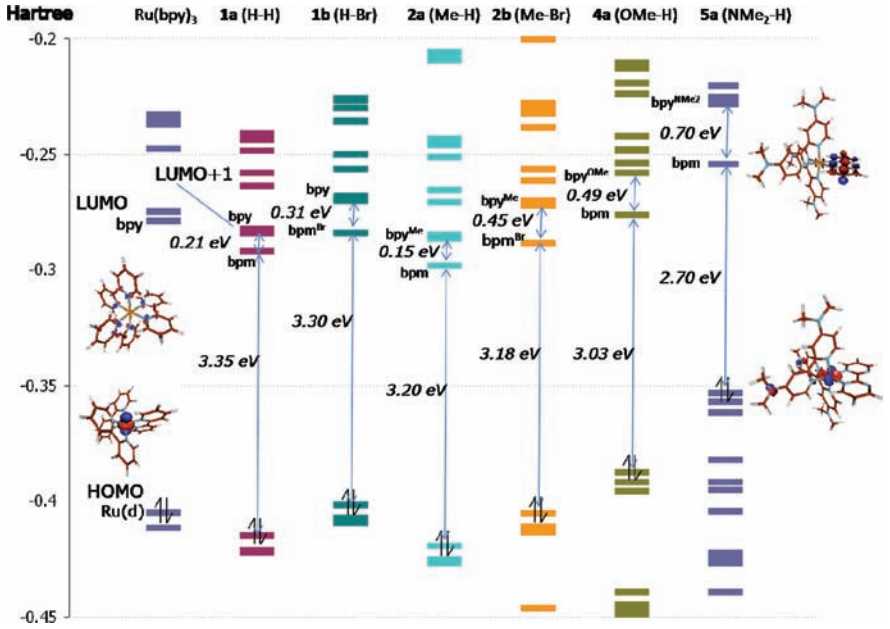

Figure 7. MO representation of $[Ru(bpy)_3]^{2+}$, **1a**, **1b**, **2a**, **2b**, **4a**, and **5a** based on DFT calculation.

Scheme 4. Plausible Photoexcited-State Structure in the Catalytic Cycle

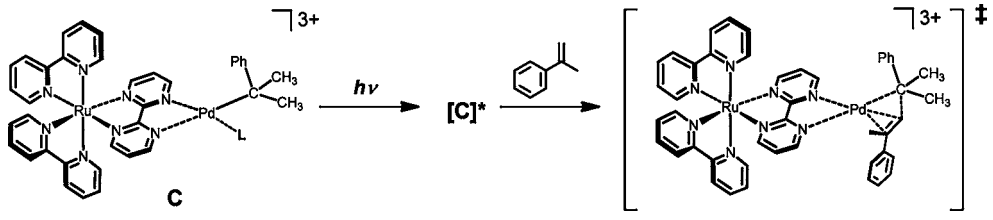

of **1a-Pd**, although less than that of **2b-Pd**. In this case, destabilization of the HOMO results in reduction of the HOMO−LUMO energy gap, resulting in a shorter excited-state lifetime. The lesser emission intensities of **4a**, **5a**, and their Pd derivatives support this. The length of the photoexcited-state lifetime seems to have an additional effect on catalytic activity.

Although we do not have any direct data for the photoexcited-state structures of the catalysts, we assume that one of the key effects is that MLCT to the bpm ligand, and the resulting trans-effect of the Pd center lead to weakening of the Pd−alkyl bond and acceleration of the insertion step (Scheme 4). Irradiation of the reaction solution results in the formation of photoexcited species such as **C*** which are related to the rate-determining step of the catalytic cycle. If the transition affects the bond strength of the Pd−$C(Me)_2$Ph bond through the trans-effect, weakening of the bond should result in rate enhancement of this key step. Thus the MLCT to bpm (not to bpy), and the resulting localization of the excited-state electron, would enhance the rate of the overall catalytic reaction. The results showing that the catalysts with larger energetic differences between the LUMO and the LUMO+1 showed higher catalytic activities strongly support this concept. Time-dependent DFT (TDDFT) calculations and time-resolved infrared spectroscopy (TRIR) studies are now ongoing to clarify the excited-state properties of the key intermediates.

3. SUMMARY

We have synthesized novel Ru(II) complexes which contain various substituents such as electron-donating Me, OMe, and NMe_2 groups on the bpy ligand, and an electron-withdrawing Br group on the bpm ligand. Their Pd−alkyl derivatives were also synthesized. The molecular structures of the complexes revealed that introduction of the substituents did not have any effect on the Ru(II) octahedral geometry if the 4,4′-position in bpy and 5,5′-position in bpm were selected for the substitutions. Similarly, the introduction of the Pd moiety did not cause steric hindrance at the Ru(II) center.

Photocatalytic activity was studied using Pd complexes containing various photosensitizing Ru(II) moieties. The introduction of an electron-donating group on the bpy and an electron-withdrawing group on bpm ligands led to drastic increase in photocatalytic activity toward α-methylstyrene oligomerization. Photochemical, electrochemical, and theoretical studies of the complexes clarified that the modification contributes to destabilization of the LUMO+1 and stabilization of the LUMO, respectively. The increase in the energy differences between the two orbitals results in preferential MLCT to the bpm ligands coordinated with the Pd center. Research into direct observation of the excited structure of the reactive intermediate in the catalysis is still ongoing; these results provide a suitable method for the molecular design of photocatalysts with high reactivity.

4. EXPERIMENTAL SECTION

General Procedures. Standard Schlenk and vacuum line techniques under N_2 atmosphere were employed for the reactions. Acetone (molecular sieves), acetonitrile (P_2O_5), and nitromethane ($CaCl_2$) were treated with appropriate drying agents, distilled, and

dx.doi.org/10.1021/ic200291t | Inorg. Chem. 2012, 51, 51−62

stored under N_2. The metal reagents, [Pd(cod)MeCl][20] and $[Ru(cod)Cl_2]_n$,[21] were prepared according to the published procedures. Other chemicals were purchased and used as received. ^1H and ^{13}C NMR spectra were recorded on Bruker AC-200, JEOL GX-270, JEOL LA-300, JEOL EX-400, and JEOL LA-500 spectrometers. Solvents for NMR measurements were dried over molecular sieves, degassed, and stored under N_2. IR, UV−vis, and steady-state emission spectra were obtained on a JASCO FT/IR 4200, JASCO V-670, and SHIMADZU RF-5300PC spectrometer, respectively. ESI-MS spectra were recorded on a ThermoQuest Finnigan LCQ Duo mass spectrometer. GC chromatography was recorded on a SHIMADZU GC-17A spectrometer. Electrochemical measurements were made with a BAS CV-50W and Hokuto Denko HZ-5000 analyzer. In the following section, $^3J_{HH}$ and $^1J_{CH}$ are abbreviated as J and J_{CH}, respectively. NMR labels for the complexes are given in Chart 1.

Chart 1. NMR Labels for Mono- and Dinuclear Ru(II) Complexes

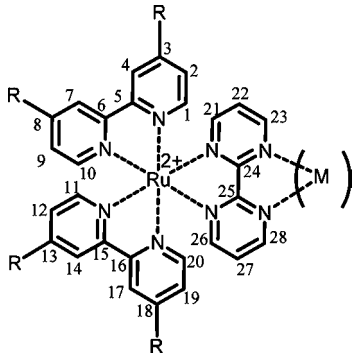

*Preparation of [(bpy^{Me})$_2$Ru(bpm)](BF$_4$)$_2$ (**2a**).* To a EtOH solution of *cis*-(bpy^{Me})$_2$RuCl$_2$·2H$_2$O[22] (250 mg, 0.434 mmol), 2,2′-bipyrimidine (bpm) (137 mg, 0.866 mmol) was added and refluxed for 5 h. After the solution was cooled to ambient temperature, excess NH_4BF_4 was added. The precipitate was collected through filtration, and the obtained solid was washed with Et_2O. The obtained solid was dissolved in CH_3CN and purified by column chromatography packed with neutral aluminum oxide (CH_3CN:CH_2Cl_2 = 1:1). The eluted red band was collected, and removal of the solvent under vacuum gave **2a** as a red solid (306 mg, 0.382 mmol, 88%). ^1H NMR (200 MHz, r.t., CD_3CN, δ /ppm): δ 9.07 (dd, J = 4.7, 2.2 Hz, 2 H, H^{23}, H^{28}), 8.37 (s, 4 H, H^4, H^7, H^{14}, H^{17}), 8.05 (dd, J = 5.8, 1.8 Hz, 2 H, H^{21}, H^{26}), 7.68 (d, J = 5.8 Hz, 2 H, H^1, H^{20}, or H^{10}, H^{11}), 7.51 (d, J = 5.8 Hz, 2 H, H^1, H^{20}, or H^{10}, H^{11}), 7.50 (t, J = 4.6 Hz, 2 H, H^{22}, H^{27}), 7.26 (d, J = 5.8 Hz, 4 H, H^2, H^9, H^{12}, H^{19}), 2.53 (s, 12 H, −CH_3). ^{13}C NMR (100 MHz, CD_3CN, r.t., δ /ppm): δ 164.0 (s, C^{24}, C^{25}), 160.2 (d, J_{CH} = 188 Hz, C^{21}, C^{26}), 158.5 (d, J_{CH} = 188 Hz, C^{23}, C^{28}), 157.3 (s, C^5, C^{16}, or C^6, C^{15}), 157.2 (s, C^5, C^{16}, or C^6, C^{15}), 152.2 (d, J_{CH} = 183 Hz, C^1, C^{20}, or C^{10}, C^{11}), 151.7 (s, C^3, C^{18}, or C^8, C^{13}), 151.6 (d, J_{CH} = 182 Hz, C^1, C^{20}, or C^{10}, C^{11}), 129.3 (d, J_{CH} = 167 Hz, C^2, C^{19} or C^9, C^{12}), 129.2 (d, J_{CH} = 167 Hz, C^2, C^{19} or C^9, C^{12}), 125.9 (d, J_{CH} = 164 Hz, C^4, C^{17} or C^7, C^{14}), 124.9 (d, J_{CH} = 174 Hz, C^{22}, C^{27}), 21.3 (q, J_{CH} = 128 Hz, -CH_3). ESI-MS: m/z = 715 [M − BF_4]$^+$, 314 [M − 2(BF_4)]$^{2+}$. HRMS (ESI-TOF, m/z): 715.1672 [M − BF_4]$^+$ (calcd for $C_{32}H_{30}N_8BF_4{}^{102}Ru$: 715.1674).

*Preparation of [(bpy^{Me})$_2$Ru(bpm)PdMe(Me$_2$CO)](BF$_4$)$_3$ (**2a-Pd**).* A CH_3NO_2 (3.5 mL) solution of [(bpy^{Me})$_2$Ru(bpm)](BF$_4$)$_2$ (**2a**) (112 mg, 0.140 mmol) and (cod)PdMeCl (44.2 mg, 0.167 mmol) was stirred under ambient temperature for 2.5 h. The solvent was removed under reduced pressure, and the residual solid was washed with Et_2O three times. The solid was dissolved in a minimum amount of CH_2Cl_2, followed by a slow addition of Et_2O, gave [(bpy^{Me})$_2$Ru(bpm)-PdMeCl](BF$_4$)$_2$ (**2a-Cl**) as a red solid (120 mg, 0.125 mmol, 89% yield). An acetone solution (8 mL) of **2a-Cl** (120 mg, 0.125 mmol) and $AgBF_4$ (28.2 mg, 0.145 mmol) was stirred under ambient temperature for 2 h. The solution was filtered through Celite and concentrated. Addition of Et_2O gave **2a-Pd** as a reddish-brown solid (178 mg, 0.167 mmol, 97% yield from **2a-Cl**, 86% overall yield). ^1H NMR (200 MHz, CD_3CN, r.t., δ /ppm): δ 9.05 (s, 2 H, H^{23}, H^{28}), 8.36 (s, 4 H, H^4, H^{17}, H^7, H^{14}), 8.21 (d, J = 4.3 Hz, 2 H, H^{21}, H^{26}), 7.74 (d, J = 5.2 Hz, 4 H, H^1, H^{20}, H^{10}, H^{11}), 7.50 (t, J = 5.2 Hz, 2 H, H^{22}, H^{27}), 7.26 (d, J = 5.2 Hz, 4 H, H^2, H^9, H^{12}, H^{19}), 2.53 (s, 12 H, bpy-CH_3), 1.05 (s, 3 H, Pd-CH_3). The proton signal of the coordinated acetone is overlapped with the residual proton signal of CD_3CN. ^{13}C NMR (125 MHz, CD_3CN, r.t., δ /ppm): δ 165.8 (s, C^{24}, C^{25}), 162.7 (d, J_{CH} = 193 Hz, C^{23}, C^{28}), 157.4 (s, C^5, C^{16}, C^6, C^{15}), 156.2 (d, J_{CH} = 196 Hz, C^{21}, C^{26}), 153.6 (d, J_{CH} = 185 Hz, C^1, C^{20} or C^{10}, C^{11}), 152.5 (s, C^3, C^{18}, C^8, C^{13}), 151.8 (d, J_{CH} = 184 Hz, C^1, C^{20} or C^{10}, C^{11}), 129.5 (d, J_{CH} = 168 Hz, C^2, C^{19}, C^9, C^{12}), 127.5 (m, C^{22}, C^{27}), 126.2 (d, J_{CH} = 162 Hz, C^4, C^7, C^{14}, C^{17}), 21.3 (q, J_{CH} = 128 Hz, bpy-CH_3), 4.1 (q, J_{CH} = 137 Hz, Pd-CH_3). Anal. Calcd for $C_{36}H_{39}N_8B_3F_{12}RuPdO$ + 2H_2O: C, 39.18; H, 3.93; N, 10.15. Found: C, 38.72; H, 3.51; N, 10.23.

*Preparation of [(bpy^{Me})$_2$Ru(bpm^{Br})](BF$_4$)$_2$ (**2b**).* To a EtOH solution of *cis*-(bpy^{Me})$_2$RuCl$_2$[9] (519 mg, 0.960 mmol), AgOTf (493 mg, 1.92 mmol) was added and stirred at ambient temperature for 5 h. The resulting solution was filtered through Celite, 5,5′-dibromo-2,2′-bipyrimidine (366 mg, 1.16 mmol) was added, and the solution was refluxed for 12 h. After the solvent was removed under reduced pressure, the solid was dissolved into EtOH. The orange-brown solid was precipitated after addition of a saturated NH_4BF_4 solution. The precipitate was filtered and crystallized from CH_2Cl_2/hexane to yield **2b** as a brownish green solid (359 mg, 0.374 mmol, 39%). ^1H NMR (200 MHz, r.t., CD_3NO_2, δ/ppm): δ 9.18 (d, J = 2.5 Hz, 2 H, H^{23}, H^{28}), 8.54 (b s, 4 H, H^4, H^7, H^{14}, H^{17}), 8.47 (d, J = 2.5 Hz, 2 H, H^{21}, H^{26}), 8.01 (d, J = 5.7 Hz, 2 H, H^1, H^{20}, or H^{10}, H^{11}), 7.66 (d, J = 5.7 Hz, 2 H, H^1, H^{20}, or H^{10}, H^{11}), 7.31 (m, 4 H, H^2, H^9, H^{12}, H^{19}), 2.53 (s, 6 H, bpy-*Me*), 2.50 (s, 6 H, bpy-*Me*). ^{13}C NMR (67.8 MHz, r.t., CD_3NO_2): 162.8 (s, C^{24}, C^{25}), 161.0 (dd, J_{CH} = 194, 4.3 Hz, C^{21}, C^{26}), 159.8 (dd, J_{CH} = 197. Four Hz, C^{23}, C^{28}), 157.7 (d, $^2J_{CH}$ = 9.8 Hz, C^5, C^6, C^{15}, C^{16}), 152.7[4] (q, $^2J_{CH}$ = 5.9 Hz, C^3, C^{18}, or C^8, C^{13}), 152.6[7] (q, $^2J_{CH}$ = 5.9 Hz, C^3, C^{18} or C^8, C^{13}), 152.4 (dd, J_{CH} = 179, $^2J_{CH}$ = 3.9 Hz, C^1, C^{20}, or C^{10}, C^{11}), 151.9 (dd, J_{CH} = 187, $^2J_{CH}$ = 6.2 Hz, C^1, C^{20}, or C^{10}, C^{11}), 129.7 (d, J_{CH} = 171 Hz, C^2, C^9, C^{12}, C^{19}), 126.2 (d, J_{CH} = 164 Hz, C^4, C^7, C^{14}, C^{17}), 124.0 (d, $^2J_{CH}$ = 5.0 Hz, C^{22}, C^{27}), 21.5 (q, J_{CH} = 132 Hz, bpy-*Me*), 21.4 (q, J_{CH} = 131.6 Hz, bpy-*Me*). ESI-MS: m/z = 873 [M − BF_4]$^+$. HRMS (ESI-TOF, m/z): 872.9867 [M − BF_4]$^+$ (calcd for $C_{32}H_{28}BBr_2F_4N_8{}^{102}Ru$: 872.9866).

*Preparation of [(bpy^{Me})$_2$Ru(bpm^{Br})PdMe(Me$_2$CO)](BF$_4$)$_3$ (**2b-Pd**).* A CH_3NO_2 (10 mL) solution of [(bpy^{Me})$_2$Ru(bpm^{Br})](BF$_4$)$_2$ (**2b**) (296 mg, 0.309 mmol) and (cod)PdMeCl (123 mg, 0.464 mmol) was stirred under ambient temperature for 2 h. The solvent was removed under reduced pressure, and the residual solid was dissolved in a minimum amount of CH_2Cl_2, followed by a slow addition of Et_2O, and gave [(bpy^{Me})$_2$Ru(bpm^{Br})PdMeCl](BF$_4$)$_2$ (**2b-Cl**) as a dark green solid (200 mg, 0.179 mmol, 58% yield). An acetone solution (15 mL) of **2b-Cl** (200 mg, 0.179 mmol) was added to an acetone solution (3.5 mL) of $AgBF_4$ (34.9 mg, 0.179 mmol) and stirred under ambient temperature for 2 h. The solution was filtered through Celite and concentrated. Addition of Et_2O gave [(bpy^{Me})$_2$Ru(bpm^{Br})PdMe-(acetone)](BF$_4$)$_3$ (**2b-Pd**) as a greenish dark-brown solid (210 mg, 0.171 mmol, 96% yield from **2b-Cl**, 55% overall yield). ^1H NMR (500 MHz, CD_3CN, r.t., δ /ppm): δ 9.12 (bs, 2 H, H^{23}, H^{28}), 8.38 (bs, 2 H, H^4, H^{17} or H^7, H^{14}), 8.36 (bs, 2 H, H^4, H^{17} or H^7, H^{14}), 8.11 (bs, 2 H, H^{21}, H^{26}), 7.72 (d, J = 3.1 Hz, 2 H, H^1, H^{20} or H^{10}, H^{11}), 7.40 (d, J = 5.5 Hz, 2 H, H^2, H^{19} or H^9, H^{12}), 7.29 (d, J = 3.7 Hz, 2 H, H^1, H^{20} or H^{10}, H^{11}), 7.23 (d, J = 4.9 Hz, 2 H, H^2, H^{19} or H^9, H^{12}) 2.56 (s, 6 H, bpy-*Me*), 2.52 (s, 6 H, bpy-*Me*), 1.06 (bs, 3 H, Pd-*Me*). Proton signal of the coordinated acetone is overlapped with the residual proton signal of CD_3CN. ^{13}C NMR (125 MHz, CD_3CN, r.t., δ /ppm): δ 162.3 (s, C^{24}, C^{25}), 160.9 (d, J_{CH} = 163.3 Hz, C^{21}, C^{26}), 159.5 (d, J_{CH} = 175.0 Hz, C^{23}, C^{28}), 157.3 (d, $^2J_{CH}$ = 7.8 Hz, C^5, C^{16} or C^6, C^{15}), 157.1 (d, $^2J_{CH}$ = 7.8 Hz, C^5, C^{16} or C^6, C^{15}), 152.8 (d, J_{CH} = 180.8 Hz, C^1, C^{20} or C^{10}, C^{11}), 152.1 (s, C^3, C^{18}, C^8, C^{13}), 151.7 (d, J_{CH} = 184.7 Hz,

dx.doi.org/10.1021/ic200291t | *Inorg. Chem.* 2012, 51, 51−62

C^1, C^{20} or C^{10}, C^{11}), 129.4 (dm, J_{CH} = 167.2 Hz, C^2, C^{19} or C^9, C^{12}), 129.2 (dm, J_{CH} = 167.2 Hz, C^2, C^{19} or C^9, C^{12}), 126.1 (d, J_{CH} = 165.3 Hz, C^4, C^7, C^{14}, C^{17}), 123.7 (m, C^{22}, C^{27}), 21.2 (q, J_{CH} = 130.3 Hz, bpy-Me), −3.3 (q, J_{CH} = 143.9 Hz, Pd-Me). Complex **2b-Pd** was too unstable for the elemental analysis.

*Preparation of [(bpy^{tBu})$_2$Ru(bpm)](BF$_4$)$_2$ (**3a**).* The procedure used for the synthesis of **2a** was applied by using *cis*-(bpy^{tBu})$_2$RuCl$_2$·2H$_2$O[9] and 2,2′-bipyrimidine as starting materials (94% yield). ^{1}H NMR (400 MHz, r.t., CD_3CN, δ /ppm): δ 9.07 (dd, J = 4.9, 2.0 Hz, 2 H, H^{23}, H^{28}), 8.49 (s, 4 H, H^4, H^7, H^{14}, H^{17}), 8.05 (dd, J = 5.8, 2.0 Hz, 2 H, H^{21}, H^{26}), 7.63 (d, J = 6.1 Hz, 2 H, H^1, H^{20}, or H^{10}, H^{11}), 7.57 (d, J = 5.9 Hz, 2 H, H^1, H^{20}, or H^{10}, H^{11}), 7.56 (t, J = 5.6 Hz, 2 H, H^{22}, H^{27}), 7.26 (dd, J = 5.4, 2.0 Hz, 4 H, H^2, H^9, H^{12}, H^{19}), 1.41 (s, 36 H, −C(C*H*$_3$)$_3$). ^{13}C NMR (100 MHz, CD_3CN, r.t., δ /ppm): δ 164.1 (s, C^{24}, C^{25}), 163.8 (s, C^3, C^8), 160.1 (d, J_{CH} = 189 Hz, C^{21}, C^{26}), 158.5 (d, J_{CH} = 189 Hz, C^{23}, C^{28}), 157.5 (s, C^5, C^{16}, or C^6, C^{15}), 157.3 (s, C^5, C^{16}, or C^6, C^{15}), 152.4 (d, J_{CH} = 183 Hz, C^1, C^{20}, or C^{10}, C^{11}), 151.8 (d, J_{CH} = 182 Hz, C^1, C^{20}, or C^{10}, C^{11}), 125.7 (d, J_{CH} = 166 Hz, C^2, C^{19} or C^9, C^{12}), 125.6 (d, J_{CH} = 166 Hz, C^2, C^{19} or C^9, C^{12}), 125.0 (d, J_{CH} = 174 Hz, C^4, C^{17}, C^7, C^{14}), 122.5 (s, J_{CH} = 162 Hz, C^{22}, C^{27}), 36.3 (s, -C(CH$_3$)$_3$), 30.4 (q, J_{CH} = 126 Hz, -C(CH$_3$)$_3$). ESI-MS: m/z = 883 [M − BF$_4$]$^+$, 398 [M − 2(BF$_4$)]$^{2+}$. Anal. Calcd for $C_{44}H_{54}N_8B_2F_8Ru$: C, 54.50; H, 5.61; N, 11.56. Found: C, 54.14; H, 5.98; N, 11.31.

*Preparation of [(bpy^{tBu})$_2$Ru(bpm)PdMe(Me$_2$CO)](BF$_4$)$_3$ (**3a-Pd**).* The procedure used for the synthesis of **2a-Pd** was applied by using [(bpy^{tBu})$_2$Ru(bpm)](BF$_4$)$_2$, (cod)PdMeCl, and AgBF$_4$ as starting materials (92% yield). ^{1}H NMR (500 MHz, CD_3CN, 243 K, δ /ppm): δ 9.05 (bs, 2 H, H^{23}, H^{28}), 8.50 (s, 4 H, H^4, H^{17}, H^7, H^{14}), 8.22 (dd, J = 5.2, 1.9 Hz, 2 H, H^{21}, H^{26}), 7.85 (d, J = 5.5 Hz, 2 H, H^1, H^{20} or H^{10}, H^{11}), 7.80 (t, J = 5.5 Hz, 2 H, H^{22}, H^{27}), 7.48 (d, J = 6.1 Hz, 2 H, H^1, H^{20} or H^{10}, H^{11}), 7.45 (dd, J = 6.1, 1.9 Hz, 2 H, H^2, H^9 or H^{12}, H^{19}), 7.42 (dd, J = 6.1, 1.9 Hz, 2 H, H^2, H^9 or H^{12}, H^{19}), 1.41 (s, 39 H, −C(CH$_3$)$_3$ and Pd-CH$_3$). The proton signal of the coordinated acetone is overlapped with the residual proton signal of CD_3CN. ^{13}C NMR (125 MHz, CD_3CN, 243 K, δ /ppm): δ 164.1 (s, C^{24}, C^{25}), 163.8 (s, C^3, C^{18} or C^8, C^{13}), 162.3 (d, J_{CH} = 194 Hz, C^{23}, C^{28}), 157.2 (s, C^5, C^{16} or C^6, C^{15}), 156.8 (s, C^5, C^{16} or C^6, C^{15}), 155.8 (d, J_{CH} = 194 Hz, C^{21}, C^{26}), 153.8 (d, J_{CH} = 183 Hz, C^1, C^{20} or C^{10}, C^{11}), 151.8 (d, J_{CH} = 183 Hz, C^1, C^{20} or C^{10}, C^{11}), 127.1 (d, J_{CH} = 174 Hz, C^{22}, C^{27}), 125.4 (d, J_{CH} = 165 Hz, C^2, C^{19}or C^9, C^{12}), 122.6 (d, J_{CH} = 165 Hz, C^2, C^{19}or C^9, C^{12}), 122.4 (d, J_{CH} = 174 Hz, C^4, C^{17}, C^7, C^{14}), 36.1 (s, -C(CH$_3$)$_3$), 30.1 (q, J_{CH} = 122 Hz, -C(CH$_3$)$_3$), 3.8 (q, J_{CH} = 137 Hz, Pd-CH$_3$). Elemental analysis was done with the CH_3CN analogue (bpy^{tBu})$_2$Ru(bpm)PdMe(MeCN)](BF$_4$)$_3$ because of its higher stability. Anal. Calcd for $C_{47}H_{60}B_3F_{12}N_9PdRu + CH_2Cl_2$: C, 44.22; H, 4.79; N, 9.67. Found: C, 43.79; H, 4.58; N, 9.56.

*Preparation of [(bpy^{tBu})$_2$Ru(bpm^{Br})](BF$_4$)$_2$ (**3b**).* The procedure used for the synthesis of **2b** was applied by using (bpy^{tBu})$_2$RuCl$_2$·2H$_2$O and 5,5′-dibromo-2,2′-bipyrimidine as starting materials (37% yield). ^{1}H NMR (300 MHz, CD_3CN, r.t., δ /ppm): δ 9.15 (d, J = 2.4 Hz, 2 H, H^{23}, H^{28}), 8.47 (d, J = 2.0, 2 H, H^4, H^{17} or H^7, H^{14}), 8.46 (d, J = 2.0 Hz, 2 H, H^4, H^{17} or H^7, H^{14}), 8.05 (d, J = 2.6 Hz, 2 H, H^{21}, H^{26}), 7.78 (d, J = 6.0 Hz, 2 H, H^1, H^{20} or H^{10}, H^{11}), 7.46 (d, J = 6.0 Hz, 2 H, H^1, H^{20} or H^{10}, H^{11}), 7.42 (dd, J = 5.9 and 2.0 Hz, 2 H, H^2, H^{19} or H^9, H^{12}), 7.40 (dd, J = 5.9 and 2.0 Hz, 2 H, H^2, H^{19} or H^9, H^{12}), 1.42 (s, 18 H, bpy-^{t}*Bu*), 1.39 (s, 18 H, bpy-^{t}*Bu*). ^{13}C NMR (125 MHz, CD_3CN, r.t., δ /ppm): δ 164.1 (s, C^3, C^{18} or C^8, C^{13}), 164.0 (s, C^3, C^{18} or C^8, C^{13}), 162.1 (dd, $^2J_{CH}$ = 8.3 and 8.3 Hz, C^{24}, C^{25}), 160.5 (d, J_{CH} = 193.0 Hz, C^{21}, C^{26}), 159.4 (d, J_{CH} = 179.5 Hz, C^{23}, C^{28}), 157.5 (d, J_{CH} = 8.7 Hz, C^5, C^{16} or C^6, C^{15}), 157.2 (d, J_{CH} = 7.8 Hz, C^5, C^{16} or C^6, C^{15}), 152.9 (d, J_{CH} = 183.1 Hz, C^1, C^{20} or C^{10}, C^{11}), 151.9 (d, J_{CH} = 182.7 Hz, C^1, C^{20} or C^{10}, C^{11}), 125.6 (dd, J_{CH} = 166.2 and 6.2 Hz, C^2, C^{19} or C^9, C^{12}), 125.5 (dd, J_{CH} = 165.4, $^2J_{CH}$ = 6.2 Hz, C^2, C^{19} or C^9, C^{12}), 123.8 (s, C^{22}, C^{27}), 122.6 (d, J_{CH} = 163.3 Hz C^4, C^7, C^{14}, C^{17}), 36.3 (s, bpy-C(CH$_3$)$_3$), 30.4 (q, J_{CH} = 125.8 Hz, bpy-C(CH$_3$)$_3$). ESI-MS: m/z = 1041 [M − BF$_4$]$^+$. Anal. Calcd for $C_{44}H_{52}B_2Br_2F_8N_8Ru + 2(H_2O)$: C, 45.42; H, 4.85; N, 9.63. Found: C, 45.29; H, 5.07; N, 9.56. HRMS (ESI-TOF, m/z): 1041.1770 [M − BF$_4$]$^+$ (calcd for $C_{44}H_{52}BBr_2F_4N_8{}^{102}Ru$: 1041.1749).

*Preparation of [(bpy^{tBu})$_2$Ru(bpm^{Br})PdMe(acetone)](BF$_4$)$_3$ (**3b-Pd**).* The procedure used for the synthesis of **2b-Pd** was applied by using [(bpy^{tBu})$_2$Ru(bpm^{Br})](BF$_4$)$_2$, (cod)PdMeCl, and AgBF$_4$ as starting materials (70% yield). ^{1}H NMR (500 MHz, CD_3CN, r.t., δ /ppm): δ 9.15 (d, J = 2.4 Hz, 2 H, H^{23}, H^{28}), 8.47 (d, J = 2.0 Hz, 2 H, H^4, H^{17} or H^7, H^{14}), 8.45 (d, J = 2.0 Hz, 2 H, H^4, H^{17} or H^7, H^{14}), 8.04 (d, J = 2.4 Hz, 2 H, H^{21}, H^{26}), 7.77 (d, J = 6.0 Hz, 2 H, H^1, H^{20} or H^{10}, H^{11}), 7.47 (d, J = 6.0 Hz, 2 H, H^2, H^{19} or H^9, H^{12}), 7.41 (dd, J = 5.9, 2.0 Hz, 2 H, H^1, H^{20} or H^{10}, H^{11}), 7.39 (dd, J = 5.9, 2.0 Hz, 2 H, H^2, H^{19} or H^9, H^{12}), 1.43 (s, 18 H, bpy-^{t}*Bu*), 1.40 (s, 18 H, bpy-^{t}*Bu*), 1.39 (s, 3 H, Pd-*Me*). Proton signal of the coordinated acetone is overlapped with the residual proton signal of CD_3CN. ^{13}C NMR (125 MHz, CD_3CN, r.t., δ /ppm): δ 164.3 (d, J_{CH} = 11.7 Hz C^3, C^{18} or C^8, C^{13}), 164.2 (d, $^2J_{CH}$ = 9.7 Hz C^3, C^{18} or C^8, C^{13}), 162.3 (s, C^{24}, C^{25}), 160.7 (d, J_{CH} = 194.4 Hz, C^{21}, C^{26}), 160.0 (d, J_{CH} = 196.4 Hz, C^{23}, C^{28}), 157.6 (d, $^2J_{CH}$ = 8.7 Hz, C^5, C^{16} or C^6, C^{15}), 157.4 (d, J_{CH} = 9.7 Hz, C^5, C^{16} or C^6, C^{15}), 153.0 (d, J_{CH} = 182.8 Hz, C^1, C^{20} or C^{10}, C^{11}), 152.0 (d, J_{CH} = 182.9 Hz, C^1, C^{20} or C^{10}, C^{11}), 125.7 (d, J_{CH} = 165.3 Hz, C^2, C^{19} or C^9, C^{12}), 125.6 (d J_{CH} = 165.3 Hz, C^2, C^{19} or C^9, C^{12}), 123.9 (s, C^{22} or C^{27}), 123.2 (s, C^{22} or C^{27}), 120.7 (s, coord. CD_3CN), 36.3 (s, bpy-C(CH$_3$)$_3$), 30.4 (dq, bpy-C(CH$_3$)$_3$), 3.3 (q, J_{CH} = 145.8 Hz, Pd-*Me*). Complex **3b-Pd** was too unstable for the elemental analysis.

*Preparation of [(bpy^{OMe})$_2$Ru(bpm)](BF$_4$)$_2$ (**4a**).* (bpy^{OMe})$_2$RuCl$_2$[23] (150 mg, 0.250 mmol) and bpm (59.0 mg, 0.373 mmol) were dissolved in EtOH (15 mL), and the solution was refluxed for 5 h. Excess amount of NH_4BF_4 was added to the solution and stirred for 12 h. The solid was precipitated and filtered, and then washed with H_2O and Et_2O. The solid was extracted with acetone and purified by Al_2O_3 column (CH_2Cl_2:CH_3CN = 3:2) to give [Ru(bpy^{OMe})$_2$(bpm)](BF$_4$)$_2$ (**4a**) (79.1 mg, 0.0914 mmol, 37% yield). ESI-MS: m/z = 779 [M − BF$_4$]$^+$. ^{1}H NMR (500 MHz, CD_3CN, r.t., δ /ppm): δ 9.02 (dd, J = 4.9 and 1.9 Hz, 2 H, H^{23}, H^{28}), 8.13 (dd, J = 5.5, 1.8 Hz, 2 H, H^{21}, H^{26}), 8.05 (d, J = 3.1 Hz, 2 H, H^4, H^{17} or H^7, H^{14}), 8.04 (d, J = 2.5 Hz, 2 H, H^4, H^{17} or H^7, H^{14}), 7.61 (d, J = 6.7 Hz, 2H, H^1, H^{20} or H^{10}, H^{11}), 7.53 (d, J = 6.1 Hz, 2H, H^1, H^{20} or H^{10}, H^{11}), 7.52 (t, J = 6.1 Hz, 2 H, H^{22}, H^{27}), 7.00 (dd, J = 6.8, 3.1 Hz, 2 H, H^2, H^{19} or H^9, H^{12}), 6.96 (dd, J = 6.7, 2.5 Hz, 2 H, H^2, H^{19} or H^9, H^{12}), 4.00 (s, 6 H, bpy-O*Me*), 3.99 (s, 6H, bpy-O*Me*). ^{13}C NMR (125 MHz, CD_3CN, r.t., δ /ppm): δ 168.2 (s, C^{24}, C^{25}), 164.7 (dd, $^2J_{CH}$ = 7.8, 9.7 Hz, C^3, C^8, C^{13}, C^{18}), 160.4 (d, J_{CH} = 186.7 Hz, C^{21}, C^{26}), 158.9 (s, C^5, C^6, C^{15}, C^{16}), 158.1 (d, J_{CH} = 198.3 Hz, C^{23}, C^{28}), 153.8 (d, J_{CH} = 182.8 Hz, C^1, C^{20} or C^{10}, C^{11}), 153.1 (d, J_{CH} = 182.8 Hz, C^1, C^{20} or C^{10}, C^{11}), 124.8 (ddd, J_{CH} = 173.1, $^2J_{CH}$ = 7.8, 3.9 Hz, C^{22}, C^{27}), 114.8 (d, J_{CH} = 167.2 Hz, C^2, C^{19} or C^9, C^{12}), 114.7 (d, J_{CH} = 167.2 Hz, C^2, C^{19} or C^9, C^{12}), 112.0[4] (dd, J_{CH} = 165.3, $^2J_{CH}$ = 9.7 Hz, C^4, C^{17} or C^7, C^{14}), 111.9[6] (dd, J_{CH} = 165.3, $^2J_{CH}$ = 9.7 Hz, C^4, C^{17} or C^7, C^{14}), 57.6 (q, J_{CH} = 145.8 Hz, bpy-OMe). Anal. Calcd for $C_{32}H_{30}B_2F_8N_8O_4Ru + 2(H_2O)$: C, 42.64; H, 3.80; N, 12.43. Found: C, 42.55; H, 3.31; N, 12.78. HRMS (ESI-TOF, m/z): 779.1459 [M − BF$_4$]$^+$ (calcd for $C_{32}H_{30}BF_4N_8O_4{}^{102}Ru$: 779.1470).

*Preparation of [(bpy^{OMe})$_2$Ru(bpm)PdMe(acetone)](BF$_4$)$_3$ (**4a-Pd**).* The procedure used for the synthesis of **2a-Pd** was applied by using [(bpy^{OMe})$_2$Ru(bpm)](BF$_4$)$_2$, (cod)PdMeCl, and AgBF$_4$ as starting materials (89% yield). ^{1}H NMR (500 MHz, CD_3CN, r.t., δ /ppm): δ 8.91 (d, J = 4.3 Hz, 2H, H^{23}, H^{28}), 8.31 (s, 2H, H^{21}, H^{26}), 8.04 (d, J = 3.1 Hz, 2 H, H^4, H^{17} or H^7, H^{14}), 8.03 (d, J = 2.5 Hz, 2 H, H^4, H^{17} or H^7, H^{14}), 7.77 (d, J = 5.5 Hz, 2 H, H^1, H^{20} or H^{10}, H^{11}), 7.70 (d, J = 6.1 Hz, 2 H, H^1, H^{20} or H^{10}, H^{11}), 7.45 (t, J = 6.1 Hz, 2 H, H^{22}, H^{27}), 7.01 (dd, J = 6.7, 2.5 Hz, 4 H, H^2, H^9, H^{12}, H^{19}), 4.01 (s, 12 H, bpy-O*Me*), 1.36 (s, 3 H, Pd-*Me*). Proton signal of the coordinated acetone is overlapped with the residual proton signal of CD_3CN. ^{13}C NMR (125 MHz, CD_3CN, r.t., δ /ppm): δ 168.7 (s, C^{24}, C^{25}), 162.6 (d, J_{CH} = 194.4 Hz, C^{21}, C^{26}), 158.8 (d, $^2J_{CH}$ = 9.7 Hz, C^5, C^6, C^{15}, C^{16}), 158.6 (d, $^2J_{CH}$ = 9.7 Hz, C^3, C^8, C^{13}, C^{18}), 155.6 (d, J_{CH} = 194.5 Hz, C^{23}, C^{28}), 155.0 (d, J_{CH} = 184.7 Hz, C^1, C^{20} or C^{10}, C^{11}), 153.1 (d, J_{CH} = 182.8 Hz, C^1, C^{20} or C^{10}, C^{11}), 127.2 (d, J_{CH} = 178.9 Hz, C^{22}, C^{27}), 114.9 (dd, J_{CH} = 169.2, $^2J_{CH}$ = 5.8 Hz, C^2, C^{19} or C^9, C^{12}), 114.8 (dd, J_{CH} = 169.2, $^2J_{CH}$ = 5.8 Hz, C^2, C^{19} or C^9, C^{12}), 112.1[6] (d, J_{CH} = 165.3 Hz, C^4, C^{17} or C^7, C^{14}), 112.1[3] (d, J_{CH} = 165.3 Hz, C^4, C^{17} or C^7,

dx.doi.org/10.1021/ic200291t | *Inorg. Chem.* 2012, 51, 51−62

C^{14}), 57.7 (q, J_{CH} = 145.8 Hz, bpy-OMe), 3.87 (q, J_{CH} = 136.1 Hz, Pd-Me). Complex **4a-Pd** was too unstable for the elemental analysis. HRMS (ESI-TOF, m/z): 1027.1016 $[M - BF_4]^+$ (calcd for $C_{35}H_{36}B_2F_8N_9O_4{}^{106}Pd^{102}Ru$: 1027.1059).

Preparation of $[(bpy^{NMe2})_2Ru(bpm)](BF_4)_2$ (**5a**). The procedure used for the synthesis of **4a** was applied by using $(bpy^{NMe2})_2RuCl_2{\cdot}2H_2O$[24] and 2,2′-bipyrimidine as starting materials (6.9% yield). ESI-MS: m/z = 831 $[M - BF_4]^+$. ^{1}H NMR (500 MHz, CD_3CN, r.t., δ /ppm): δ 8.96 (dd, J = 4.9, 2.4 Hz, 2 H, H^{23}, H^{28}), 8.21 (dd, J = 5.5, 1.9 Hz, 2 H, H^{21}, H^{26}), 7.53 (d, J = 2.5 Hz, 2 H, H^4, H^{17} or H^7, H^{14}), 7.51 (d, J = 2.5 Hz, 2 H, H^4, H^{17} or H^7, H^{14}), 7.46 (dd, J = 4.9, 4.9 Hz, 2 H, H^{22}, H^{27}), 7.19 (d, J = 6.8 Hz, 2 H, H^1, H^{20} or H^{10}, H^{11}), 7.16 (d, J = 6.8 Hz, 2 H, H^1, H^{20} or H^{10}, H^{11}), 6.60 (dd, J = 6.7, 3.1 Hz, 2 H, H^2, H^{19} or H^9, H^{12}), 6.50 (dd, J = 6.7, 3.1 Hz, 2 H, H^2, H^{19} or H^9, H^{12}), 3.13 (s, 12 H, bpy-N*Me*), 3.11 (s, 12 H, bpy-N*Me*). ^{13}C NMR (125 MHz, CD_3CN, r.t., δ /ppm): δ 165.6 (dd, $^2J_{CH}$ = 9.7, 9.7 Hz, C^{24}, C^{25}), 160.1 (d, J_{CH} = 184.7 Hz, C^{21}, C^{26}), 157.6 (d, $^2J_{CH}$ = 9.7 Hz, C^3, C^{18} or C^8, C^{13}), 157.5 (d, $^2J_{CH}$ = 9.7 Hz, C^3, C^{18} or C^8, C^{13}), 156.7 (d, J_{CH} = 188.6 Hz, C^1, C^{20} or C^{10}, C^{11}), 156.6 (d, J_{CH} = 192.5 Hz, C^1, C^{20} or C^{10}, C^{11}), 155.6[3] (s, C^5, C^{16} or C^6, C^{15}), 155.5[9] (s, C^5, C^{16} or C^6, C^{15}), 150.8 (d, J_{CH} = 178.9 Hz, C^2, C^{19} or C^9, C^{12}), 150.0 (d, J_{CH} = 176.9 Hz, C^2, C^{19} or C^9, C^{12}), 124.4 (ddd, J_{CH} = 173.1, $^2J_{CH}$ = 5.8, 5.8 Hz, C^{22}, C^{27}), 110.3 (d, J_{CH} = 165.3 Hz, C^{23}, C^{28}), 106.8[4] (dd, J_{CH} = 169.2, $^2J_{CH}$ = 3.9 Hz, C^4, C^{17} or C^7, C^{14}), 106.7[8] (dd, J_{CH} = 161.4, $^2J_{CH}$ = 3.9 Hz, C^4, C^{17} or C^7, C^{14}), 40.0 (q, J_{CH} = 136.1 Hz, bpy-N*Me*). Anal. Calcd for $C_{36}H_{42}B_2F_8N_{12}Ru + H_2O$: C, 46.22; H, 4.74; N, 17.97. Found: C, 46.25; H, 4.56; N, 18.09. HRMS (ESI-TOF, m/z): 831.2738 $[M - BF_4]^+$ (calcd for $C_{36}H_{42}BF_4N_{12}{}^{102}Ru$: 831.2737).

Preparation of $[(bpy^{NMe2})_2Ru(bpm)PdMe(acetone)](BF_4)_3$ (**5a-Pd**). The procedure used for the synthesis of **2a-Pd** was applied by using $[Ru(bpy^{NMe2})_2(bpm)](BF_4)_2$, (cod)PdMeCl, and $AgBF_4$ as starting materials (83% yield). ^{1}H NMR (500 MHz, CD_3CN, r.t., δ /ppm): δ 8.81 (d, J = 4.3 Hz, 2 H, H^{23}, H^{28}), 8.39 (d, J = 5.5 Hz, 2 H, H^{21}, H^{26}), 7.71 (dd, J = 5.5, 5.5 Hz, 2 H, H^{22}, H^{27}), 7.52 (d, J = 2.5 Hz, 2 H, H^4, H^{17} or H^7, H^{14}), 7.49 (d, J = 2.5 Hz, 2 H, H^4, H^{17} or H^7, H^{14}), 7.20 (d, J = 6.8 Hz, 2 H, H^1, H^{20} or H^{10}, H^{11}), 7.09 (d, J = 6.7 Hz, 2 H, H^1, H^{20} or H^{10}, H^{11}), 6.60 (dd, J = 6.7, 3.1 Hz, 2 H, H^2, H^{19} or H^9, H^{12}), 6.53 (dd, J = 6.7, 2.5 Hz, 2H, H^2, H^{19} or H^9, H^{12}), 3.14 (s, 12 H, bpy-N*Me*), 3.13 (s, 12 H, bpy-N*Me*), 1.34 (s, 3 H, Pd-*Me*). The proton signal of the coordinated acetone is overlapped with the residual proton signal of CD_3CN. ^{13}C NMR (125 MHz, CD_3CN, r.t., δ /ppm): δ 167.1 (s, C^{24}, C^{25}), 160.1 (d, J_{CH} = 192.5 Hz, C^{21}, C^{26}), 157.2 (s, C^3, C^{18} or C^8, C^{13}), 157.1 (s, C^3, C^{18} or C^8, C^{13}), 155.9 (s, C^5, C^{16} or C^6, C^{15}), 155.8 (s, C^5, C^{16} or C^6, C^{15}), 153.9 (d, J_{CH} = 192.5 Hz, C^1, C^{10}, C^{11}, C^{20}), 151.8 (d, J_{CH} = 180.8 Hz, C^2, C^{19} or C^9, C^{12}), 149.7 (d, J_{CH} = 178.9 Hz, C^2, C^{19} or C^9, C^{12}), 126.7 (d, J_{CH} = 176.9 Hz, C^{22}, C^{27}), 110.4 (d, J_{CH} = 167.2 Hz, C^4, C^{17} or C^7, C^{14}), 110.2 (d, J_{CH} = 167.2 Hz, C^4, C^{17} or C^7, C^{14}), 106.9 (d, J_{CH} = 161.4 Hz, C^{23}, C^{28}), 40.0 (q, J_{CH} = 138.0 Hz, bpy-N*Me*), 3.65 (q, J_{CH} = 136.1 Hz, Pd-Me). Complex **5a-Pd** was too unstable for the elemental analysis. HRMS (ESI-TOF, m/z): 1080.2205 $[M - BF_4 + H]^+$ (calcd for $C_{39}H_{48}B_2F_8N_{13}{}^{106}Pd^{102}Ru$: 1080.2403).

Electrochemical Measurements. CV measurements were performed with a Pt electrode for CH_3CN solutions of the samples (ca. 2 $\times$ 10^{-3} M) in the presence of an electrolyte (0.1 M $[Bu_4N]BF_4$) at ambient temperature under an inert atmosphere. The scan rates were 100 mV/s. After the measurements, ferrocene (Fc) was added to the mixture, and the potentials were calibrated with respect to the Fc/Fc^+ redox couple.

DFT Calculations. DFT calculations were performed using the Gaussian 03[18] and Gaussian 09[19] quantum chemistry program package at the B3LYP[25,26]/LanL2DZ[27] level. Ru atoms have been described with a LanL2DZ basis set of valence double-ζ quality including the relativistic effective core potential of Hay and Wadt.[28−30] The 6-31G+ split-valence basis set is used on the nitrogen atoms coordinated to the Ru atom, the 6-31G basis set is used on the Br atoms on the bpm ligand, and the 3-21G basis set on the others. The HOMO and LUMO energies were determined by using minimized singlet geometries to approximate the ground state.

Crystal Structure Determination. The crystallographic data and the results of the structure refinements are summarized in Table 1. In the reduction of data, Lorentz and polarization corrections and empirical absorption corrections were made.[31] The structures were solved by a combination of the direct methods (SHELXS-86)[32] and Fourier synthesis (DIRDIF94).[33] Unless otherwise stated, all non-atoms were refined anisotropically, methyl H atoms were refined using riding models, and other H atoms were fixed at the calculated positions.

Photochemical Reaction. Typical reaction procedures: To a CD_3NO_2 (or CH_3NO_2) solution (1.0 mL) of **2b-Pd** (15 mg, 0.012 mmol) was added α-methylstyrene (0.6 mmol, s/c = 50) and cyclooctane (10.0 μL, as an internal standard). The solution was divided into two 5ϕ glass tubes; one for the irradiation and the other for the dark reaction which was foiled with an aluminum sheet. The two samples were placed at a distance of 10 cm from a Xe lamp (150 W, with a L42 cutoff filter (λ > 420 nm)). The reaction was followed by ^{1}H NMR and/or GC after appropriate time intervals.

■ ASSOCIATED CONTENT

Supporting Information

X-ray crystallographic data for **2a**, **2b**, **3b**, **4a**, and **2a-Pd** in CIF format. Tables of crystal data, bond distances, and bond angles for **2a**, **2b**, **3b**, **4a**, and **2a-Pd**, and Cartesian coordinates and absolute energies for all computed structures. UV−vis spectra of **1a/b-Pd**, **2a/b-Pd**, **3a/b-Pd**, **4a-Pd**, and **5a-Pd**. Plausible reaction mechanism of the catalytic reaction of α-methylstyrene, and plausible reaction mechanism of formation of trimers and tetramers in the catalysis. GCMS and GC charts of the α-methylstyrene oligomers. CV charts of the dinuclear complexes **1a-Pd**, **2a-Pd**, **3a-Pd**, **4a-Pd**, and **5a-Pd**. ^{1}H NMR charts of **2a/b**, **3a/b**, **4a**, and **5a**, and those of the corresponding dinuclear complexes. This material is available free of charge via the Internet at http://pubs.acs.org.

■ AUTHOR INFORMATION

Corresponding Author

*E-mail: inagaki.a.aa@m.titech.ac.jp (A.I.), makita@res.titech.ac.jp (M.A.).

■ ACKNOWLEDGMENTS

This research was financially supported by the Japan Society for Promotion of Science and Technology (Grant-in-Aid for Young Scientists (B): No. 16750046), the Hayashi Memorial Foundation for Female Natural Scientists, and the Japan Science and Technology Agency (PRESTO (Precursory Research for Embryonic Science and Technology; A.I.), which are gratefully acknowledged.

■ DEDICATION

The authors would like to dedicate this manuscript to Prof. Le Bozec on the occasion of his 60th birthday.

■ REFERENCES

(1) (a) Karl, T. R.; Trenberth, K. E. *Science* **2003**, *302*, 1719. (b) Akimoto, H. *Science* **2003**, *302*, 1716. (c) Rahmstorf, S.; Cazenave, A.; Church, J. A.; Hansen, J. E.; Keeling, R. F.; Parker, D. E.; Somerville, R. C. J. *Science* **2007**, *316*, 709.

(2) (a) Weiss, J. *Nature* **1938**, *141*, 248. (b) Pascal, A. A.; Liu, Z.; Broess, K.; van Oort, B.; van Amerongen, H.; Wang, C.; Horton, P.; Robert, B.; Chang, W.; Ruban, A. *Nature* **2005**, *436*, 134.

(3) (a) Collings, A., Critchley, C., Eds.; *Artificial photosynthesis*; Wiley-VCH: Weinheim, Germany, 2005. (b) Meyer, T. J. *Acc. Chem. Res.* **1989**, *22*, 163. (c) Armaroli, N.; Balzani, V. *ChemSusChem* **2011**, *4*, 21. (d) Vogler, A.; Kunkely, H. *Inorg. Chem. Commun.* **2011**, *14*, 96.

(e) Cogdell, R. J.; Brotosudarmo, T. H. P.; Gardiner, A. T.; Sanchez, P. M.; Cronin, L. *Biofuels* **2010**, *1*, 861. (f) Yagi, M.; Toda, M.; Yamada, S.; Yamazaki, H. *Chem. Commun.* **2010**, *46*, 8594. (g) McDaniel, N. D.; Bernhard, S. *Dalton Trans.* **2010**, *39*, 10021. (h) McCormick, T. M.; Calitree, B. D.; Orchard, A.; Kraut, N. D.; Bright, F. V.; Detty, M. R.; Eisenberg, R. *J. Am. Chem. Soc.* **2010**, *132*, 15480.

(4) (a) Sauvage, J.-P.; Collin, J.-P.; Chambron, J.-C.; Guillerez, S.; Balzani, V.; Barigelletti, F.; De Cola, L.; Flamigni, L. *Chem. Rev.* **1994**, *94*, 993 , and references therein. (b) Balzani, V.; Scandola, F. *Supramolecular Photochemistry*; Horwood: Chichester, England, 1990. (c) Denti, G.; Serroni, S.; Campagna, S.; Ricevuto, V.; Balzani, V. *Coord. Chem. Rev.* **1991**, *111*, 227. (d) Denti, G.; Campagna, S.; Sabatino, L.; Lerroni, S.; Ciano, M.; Balzani, V. *Inorg. Chem.* **1990**, *29*, 4750.

(5) (a) Balzani, V.; Juris, A.; Venturi, M.; Campagna, S.; Serroni, S. *Chem. Rev.* **1996**, *96*, 759 , and references therein. (b) Schubert, U. S.; Eschbaumer, C. *Angew. Chem., Int. Ed.* **2002**, *41*, 2892. (c) Polson, M. I. J.; Hanan, G. S.; Nicholas, J. T.; Hasenknopf, B.; Thouvenot, R. *Chem. Commun.* **2004**, 1314. (d) Weldon, S.; Hammarström, L.; Mukhtar, E.; Hage, R.; Gunneweg, E.; Haasnoot, J. G.; Reedijk, J.; Browne, W. R.; Guckian, A. L.; Vos, J. G. *Inorg. Chem.* **2004**, *43*, 4471. (e) Rau, S.; Walther, D.; Vos, J. G. *Dalton Trans.* **2007**, *9*, 915.

(6) (a) Osawa, M.; Hoshino, M.; Wakatsuki, Y. *Angew. Chem., Int. Ed.* **2001**, *40*, 3472. (b) Yam, V. W.-W.; Lee, V. W.-M.; Cheung, K.-K. *Organometallics* **1997**, *16*, 2833. (c) Ozawa, H.; Haga, M.; Sakai, K. *J. Am. Chem. Soc.* **2006**, *128*, 4926. (d) Catalytic photoreduction on Ni: Kimura, E.; Bu, X.; Shionoya, M.; Wada, S.; Maruyama, S. *Inorg. Chem.* **1992**, *31*, 4542. (e) Takeda, H.; Koike, K.; Inoue, H.; Ishitani, O. *J. Am. Chem. Soc.* **2008**, *130*, 2023. (f) Rau, S.; Schafer, B.; Gleich, D.; Anders, E.; Rudolph, M.; Friedrich, M.; Gorls, H.; Henry, W.; Vos, J. G. *Angew. Chem., Int. Ed.* **2006**, *45*, 6215. (g) Miyake, Y.; Nakajima, K.; Sasaki, K.; Saito, R.; Nakanishi, H.; Nishibayashi, Y. *Organometallics* **2009**, *28*, 5240.

(7) Inagaki, A.; Akita, M. *Coord. Chem. Rev.* **2010**, *254*, 1220.

(8) Inagaki, A.; Yatsuda, S.; Edure, S.; Suzuki, A.; Takahashi, T.; Akita, M. *Inorg. Chem.* **2007**, *46*, 2432.

(9) Ji, Z.; Huang, S. D.; Guadalupe, A. R. *Inorg. Chim. Acta* **2000**, *305*, 127.

(10) Inagaki, A.; Edure, S.; Yatsuda, S.; Akita, M. *Chem. Commun.* **2005**, 5468.

(11) (a) Inagaki, A.; Nakagawa, H.; Akita, M.; Inoue, K.; Sakai, M.; Fujii, M. *Dalton Trans.* **2008**, 6709. (b) Murata, K.; Ito, M.; Inagaki, A.; Akita, M. *Chem. Lett.* **2010**, *39*, 915.

(12) Johnson, L. K.; Killian, C. M.; Brookhart, M. *J. Am. Chem. Soc.* **1995**, *117*, 6414.

(13) (a) Rix, F. C.; Brookhart, M.; White, P. S. *J. Am. Chem. Soc.* **1996**, *118*, 4746. (b) Mecking, S.; Johnson, L. K.; Wang, L.; Brookhart, M. *J. Am. Chem. Soc.* **1998**, *120*, 888. (c) Shultz, C. S.; Ledford, J.; DeSimone, J. M.; Brookhart, M. *J. Am. Chem. Soc.* **2000**, *122*, 6531. (d) Tempel, D. J.; Johnson, L. K.; Huff, R. L.; White, P. S.; Brookhart, M. *J. Am. Chem. Soc.* **2000**, *122*, 6686.

(14) On the basis of GCMS data. See Supporting Information for the mechanisms of formation of dimer, trimers, and tetramers (Supporting Information, Scheme S1−S3).

(15) Rillema, D. P.; Mack, K. B. *Inorg. Chem.* **1982**, *21*, 3849.

(16) Rillema, D. P.; Allen, G.; Meyer, T. J.; Conrad, D. *Inorg. Chem.* **1983**, *22*, 1617.

(17) (a) D'Angelantonio, M.; Mulazzani, W. G.; Venturi, M.; Ciano, M.; Hoffman, M. Z. *J. Phys. Chem.* **1991**, *95*, 5121. (b) Záliś, S.; Krejčík, M.; Drchal, V.; Vlčk, A. A. *Inorg. Chem.* **1995**, *34*, 6008.

(18) Frisch, M. J.; Trucks, G. W.; Schlegel, H. B.; Scuseria, G. E.; Robb, M. A.; Cheeseman, J. R.; Montgomery, Jr., J. A.; Vreven, T.; Kudin, K. N.; Burant, J. C.; Millam, J. M. S.; Iyengar, S.; Tomasi, J.; Barone, V.; Mennucci, B.; Cossi, M.; Scalmani, G.; Rega, N.; Petersson, G. A.; Nakatsuji, H.; Hada, M.; Ehara, M.; Toyota, K.; Fukuda, R.; Hasegawa, J.; Ishida, M.; Nakajima, T.; Honda, Y.; Kitao, O.; Nakai, H.; Klene, M.; Li, X.; Knox, J. E.; Hratchian, H. P.; Cross, J. B.; Bakken, V.; Adamo, C.; Jaramillo, J.; Gomperts, R.; Stratmann, R. E.; Yazyev, O.; Austin, A. J.; Cammi, R.; Pomelli, C.; Ochterski, J. W.; Ayala, P. Y.; Morokuma, K.; Voth, G. A.; Salvador, P.; Dannenberg, J. J.; Zakrzewski, V. G.; Dapprich, S.; Daniels, A. D.; Strain, M. C.; Farkas, O.; Malick, D. K.; Rabuck, A. D.; Raghavachari, K.; Foresman, J. B.; Ortiz, J. V.; Cui, Q.; Baboul, A. G.; Clifford, S.; Cioslowski, J.; Stefanov, B. B.; Liu, G.; Liashenko, A.; Piskorz, P.; Komaromi, I.; Martin, R. L.; Fox, D. J.; Keith, T.; Al-Laham, M. A.; Peng, C. Y.; Nanayakkara, A.; Challacombe, M.; Gill, P. M. W.; Johnson, B.; Chen, W.; Wong, M. W.; Gonzalez, C.; Pople, A. J. *Gaussian 03*, Revision E.01; Gaussian, Inc.: Wallingford, CT, 2004.

(19) Frisch, M. J.; Trucks, G. W.; Schlegel, H. B.; Scuseria, G. E.; Robb, M. A.; Cheeseman, J. R.; Scalmani, G.; Barone, V.; Mennucci, B.; Petersson, G. A.; Nakatsuji, H.; Caricato, M.; Li, X.; Hratchian, H. P.; Izmaylov, A. F.; Bloino, J.; Zheng, G.; Sonnenberg, J. L.; Hada, M.; Ehara, M.; Toyota, K.; Fukuda, R.; Hasegawa, J.; Ishida, M.; Nakajima, T.; Honda, Y.; Kitao, O.; Nakai, H.; Vreven, T.; Montgomery, Jr., J. A.; Peralta, J. E.; Ogliaro, F.; Bearpark, M.; Heyd, J. J.; Brothers, E.; Kudin, K. N.; Staroverov, V. N.; Keith, T.; Kobayashi, R.; Normand, J.; Raghavachari, K.; Rendell, A.; Burant, J. C.; Iyengar, S. S.; Tomasi, J.; Cossi, M.; Rega, N.; Millam, J. M.; Klene, M.; Knox, J. E.; Cross, J. B.; Bakken, V.; Adamo, C.; Jaramillo, J.; Gomperts, R.; Stratmann, R. E.; Yazyev, O.; Austin, A. J.; Cammi, R.; Pomelli, C.; Ochterski, J. W.; Martin, R. L.; Morokuma, K.; Zakrzewski, V. G.; Voth, G. A.; Salvador, P.; Dannenberg, J. J.; Dapprich, S.; Daniels, A. D.; Farkas, O.; Foresman, J. B.; Ortiz, J. V.; Cioslowski, J.; Fox, D. J. *Gaussian 09*, Revision B.01; Gaussian, Inc.: Wallingford, CT, 2010.

(20) Rülke, R. E.; Ernsting, J. M.; Spek, A. L.; Elsevier, C. J.; van Leeuwen, P. W. N. M.; Vrieze, K. *Inorg. Chem.* **1993**, *32*, 5769.

(21) Doi, T.; Nagamiya, H.; Kokubo, M.; Hirabayashi, K.; Takahashi, T. *Tetrahedron* **2002**, *58*, 2957.

(22) Sullivan, B. P.; Salmon, D. J.; Meyer, T. J. *Inorg. Chem.* **1978**, *17*, 3334.

(23) Synthesized using 4,4′-dimethoxy-2,2′-bipyridyl and $[Ru(cod)Cl_2]_n$.

(24) Synthesized according to ref 22 using 4,4′-dimethylamino-2,2′-bipyridyl and $RuCl_3 \cdot 3H_2O$.

(25) (a) Becke, A. D. *Phys. Rev. A* **1988**, *38*, 3098. (b) Becke, A. D. *J. Chem. Phys.* **1993**, *98*, 5648.

(26) Lee, C.; Yang, W.; Parr, R. G. *Phys. Rev. B* **1988**, *37*, 785.

(27) Dunning, T. H., Jr.; Hay, P. J. In *Modern Theoretical Chemistry*; Schaefer, H. F., III, Ed.; Plenum: New York, 1976; pp 1−28.

(28) Hay, P. J.; Wadt, W. R. *J. Chem. Phys.* **1985**, *82*, 270.

(29) Hay, P. J.; Wadt, W. R. *J. Chem. Phys.* **1985**, *82*, 299.

(30) Wadt, W. R.; Hay, P. J. *J. Chem. Phys.* **1985**, *82*, 284.

(31) Higashi, T. *ABSCOR, Program for absorption correction*; Rigaku Corp.: Tokyo, Japan, 1995.

(32) (a) Sheldrick, G. M. *SHELXS-86, Program for crystal structure determination*; University of Göttingen: Göttingen, Germany, 1986. (b) Sheldrick, G. M. *SHELXL-97, Program for crystal structure refinement*; University of Göttingen: Göttingen, Germany, 1997.

(33) Beurskens, P. T.; Admiraal, G.; Beurskens, G.; Bosman, W. P.; de Gelder, R.; Israel, R.; Smits, J. M. M. *The DIRDIF-99 program system*, Technical Report of the Crystallography Laboratory; University of Nijmegen: Nijmegen, The Netherlands, 1999.